AD-A096 344 OHIO STATE UNIV COLUMBUS ELECTROSCIENCE LAB F/G 17/9
SURFACE SHIP TARGET CLASSIFICATION USING H.F. MULTI-FREQUENCY R--ETC(U)
MAY 80 H F WALTON, J D YOUNG N00014-79-C-0882
UNCLASSIFIED ESL-712352-1 NL

1 OF 1
AD A
096344

END
DATE
FILMED
4-81
DTIC

LEVEL II (12)

OSU

The Ohio State University

SURFACE SHIP TARGET CLASSIFICATION USING H.F. MULTI-FREQUENCY RADAR

E. K. Walton and J. D. Young

The Ohio State University

ElectroScience Laboratory

Department of Electrical Engineering
Columbus, Ohio   43212

FINAL REPORT 712352-1

May 1980

**DTIC
ELECTE
S MAR 1 6 1981**

A

NOTICES

When Government drawings, specifications, or other data are used for any purpose other than in connection with a definitely related Government procurement operation, the United States Government thereby incurs no responsibility nor any obligation whatsoever, and the fact that the Government may have formulated, furnished, or in any way supplied the said drawings, specifications, or other data, is not to be regarded by implication or otherwise as in any manner licensing the holder or any other person or corporation, or conveying any rights or permission to manufacture, use, or sell any patented invention that may in any way be related thereto.

REPORT DOCUMENTATION PAGE		READ INSTRUCTIONS BEFORE COMPLETING FORM
1 REPORT NUMBER	2. GOVT ACCESSION NO. AD-A096 344	3. RECIPIENT'S CATALOG NUMBER
4. TITLE *(and Subtitle)* SURFACE SHIP TARGET CLASSIFICATION USING H.F. MULTI-FREQUENCY RADAR.		5. TYPE OF REPORT & PERIOD COVERED Final Report
		6. PERFORMING ORG. REPORT NUMBER ESL-712352-1
7. AUTHOR(s) F. K. Walton and J. D. Young		8. CONTRACT OR GRANT NUMBER(s) Contract N00014-79-C-0882
9 PERFORMING ORGANIZATION NAME AND ADDRESS The Ohio State University ElectroScience Laboratory, Department of Electrical Engineering, Columbus, Ohio 43212		10. PROGRAM ELEMENT, PROJECT, TASK AREA & WORK UNIT NUMBERS
11. CONTROLLING OFFICE NAME AND ADDRESS Dept. of the Navy, Office of Naval Research 800 North Quincy Street Arlington, Virginia 22217		12. REPORT DATE May 1980
		13. NUMBER OF PAGES 69
14 MONITORING AGENCY NAME & ADDRESS *(If different from Controlling Office)*		15. SECURITY CLASS. *(of this report)* Unclassified
		15a. DECLASSIFICATION DOWNGRADING SCHEDULE

16. DISTRIBUTION STATEMENT *(of this Report)*

17. DISTRIBUTION STATEMENT *(of the abstract entered in Block 20, If different from Report)*

18. SUPPLEMENTARY NOTES

19 KEY WORDS *(Continue on reverse side if necessary and identify by block number)*

H.F. Radar	Classification
OTH	Identification
Nearest neighbor	Ships
Time domain	Ramp response

20 ABSTRACT *(Continue on reverse side if necessary and identify by block number)*

A number of studies leading to the development of ship target identification from the return from High Frequency Over the Horizon (HF OTH) radar returns were implemented.

All of the studies used data from an available data base where measurements were made of scale models on a ground plane. The frequencies used were consistent with the HF band (2-25 MHz in this case).

DD FORM 1473 EDITION OF 1 NOV 65 IS OBSOLETE
1 JAN 73

20.

The work reported on here is the initial phase of the research, and the data base was not directly usable for the testing of specific algorithms for the identification of surface ships in general. The data base was used instead to test the general identifiability of surface ships using HF OTH radar returns.

Nearest neighbor techniques and hyperline techniques were used to measure the clustering and the separation of the amplitude and phase data from the ship models in hyperspace (i.e., parameter space). Ramp response curves and pole extraction techniques were used to indicate the source of and reliability of the features found in the target return data. It was shown that the OTH returns can be expected to be inherently useful for the identification of ships.

ACKNOWLEDGMENT

TABLE OF CONTENTS

I.   INTRODUCTION

The long range goal of this research is to develop techniques
for detecting and identifying (or classifying) ship targets using H.F.
Over the Horizon radar (OTH). For the period covered in this report,
(the initial phase) several specific studies were undertaken. The
general identifiability of naval surface ships using H.F. radar was
studied first. This was a study of the behavior of an available data
set from the point of view of radar target classification. In this
sense, it was not restricted to a study of the performance of any specific
target classification algorithm. It was, rather, a quantitative appraisal
of the overall usefulness of H.F. radar returns for target classification.
Two techniques were used for this identifiability study. The nearest
neighbor technique was used to study the clustering property of the
data in multi-dimensional space, while the concept of the displacement
and skew of lines in multidimensional space (hyperlines) was used to
study the separability of the data. Time domain and resonant pole
techniques were also implemented and applied to the available data
base.

The results of these studies indicate that data from H.F. radar
systems are useful for ship target classification. In the language
of pattern recognition, the data were shown to cluster in hyperspace
and the clusters were shown to be separable. The time domain studies
were used to show that the main contributors to the backscatter features
are large significant ship structures such as the bridge geometry.
A quantitative measure of these statements will be given.

II.   DATA BASE

The automatic identification or classification of an unknown
member (ship) of a class (of ships) based on various subsets of a set
of features (measured cross section and phase vs. H.F. frequency) was
studied. The first study undertaken was to measure the inherent identi-

1

fiability of ships based on H.F. OTH radar returns. Once this property has been answered quantitatively, the development of specific applicable algorithms and their optimization can proceed. Both classifiability tests and the testing of specified classification algorithms require a data base which is representative of the data to be expected in practice. This classifiability study can work with a relatively small data set.

A set of radar backscatter measurements made by the Ohio State University ElectroScience Laboratory of scale models of ships was used as the data base for the studies reported here [1,2,3]. A summary of the data base is shown in Table 1. In each case, scale models of the

TABLE 1

OSU DATA BASE (1979)

| SHIP	SCALE	TYPE	SCALED F_0 (mHz)	# OF HARMONICS
Midway	(1:500)	Carrier	2.17	10
Missouri	(1:500)	Battleship	2.17	10
Missouri	(1:700)	Battleship	1.55	10
Sverdlov	(1:500)	Cruiser	2.17	10
Bismark	(1:700)	Battleship	1.55	10
Mogami	(1:700)	Heavy Cruiser	1.55	10
Hayanami	(1:700)	Destroyer	1.55	10
Shimokaze	(1:700)	Destroyer	1.55	10

All ships measured at bow, stern, port, and starboard aspect angles.

The Missouri (1:700) and the Sverdlov were measured at 5° aspect angle increments about the bow, stern, and starboard aspects.

2

listed ships were measured with a 29° elevation angle using a multifrequency bistatic radar system (1). The models were placed on a conducting ground plane. Measurements at 5° aspect angle increments were made for the Sverdlov and the Missouri as shown. The scaled fundamental frequency is shown in the table. Ten harmonically related measurements were made of the absolute cross section and the absolute phase (relative to a point defined at the center of the hull of the ship). As can be seen, these measurements (scaled) cover a large part of the H.F. band. A photograph of these ship models is given (Photograph 1). It is important to note that these ships are all generally of the same size, and that the size of a particular ship will not be the determining characteristic in the tests to be performed on the data.

The data for the Missouri (1:700) and the Sverdlov were used for the identifiability testing since a much larger set of aspect angles was available for them. An example set of data comprising one frequency scan is shown in Figure 1. This is a phasor representation of the measured amplitude square root of ($\sqrt{cross\ section}$ (cm)) and absolute phase of the Sverdlov at an aspect angle of 5°. The entire data base is given in Appendix A in this compact phasor plot form. Study of the data in the appendix have shown several interesting properties.

First note that as the aspect angle of a particular ship changes by 5 or 10 degrees, the position in phasor space of harmonic N (N = 1 to 5) remains relatively fixed (compared to the corresponding phasor position of the data from the second ship). For both ships, the broadside amplitudes tend to be $\approx$ 4 times larger than the bow and stern amplitudes. Distinct differences in the behavior of the Sverdlov data as compared with the Missouri data can also be seen in the phasor plots. The techniques used in the next three sections of this report can be used to quantify this observation.

3
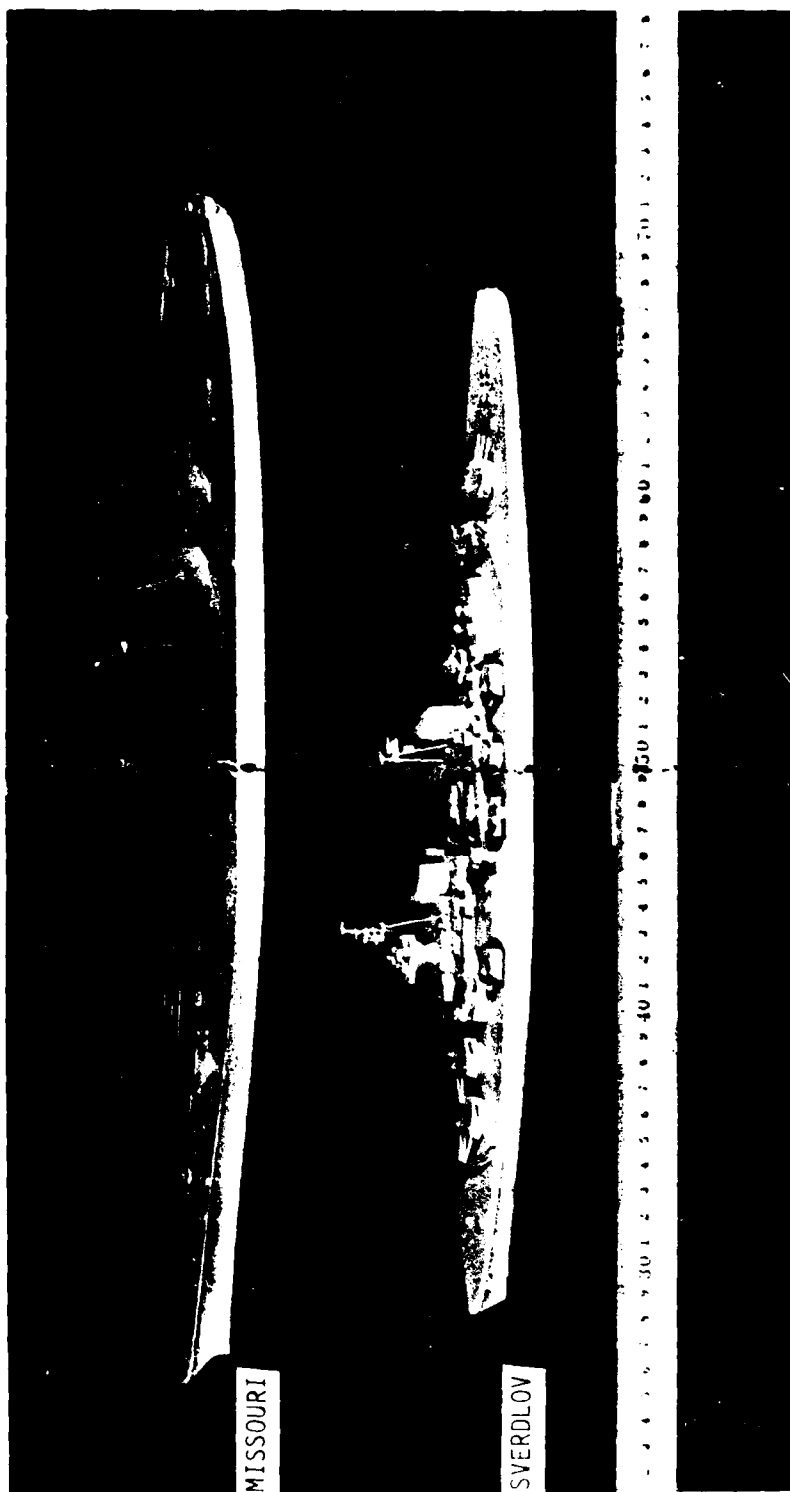
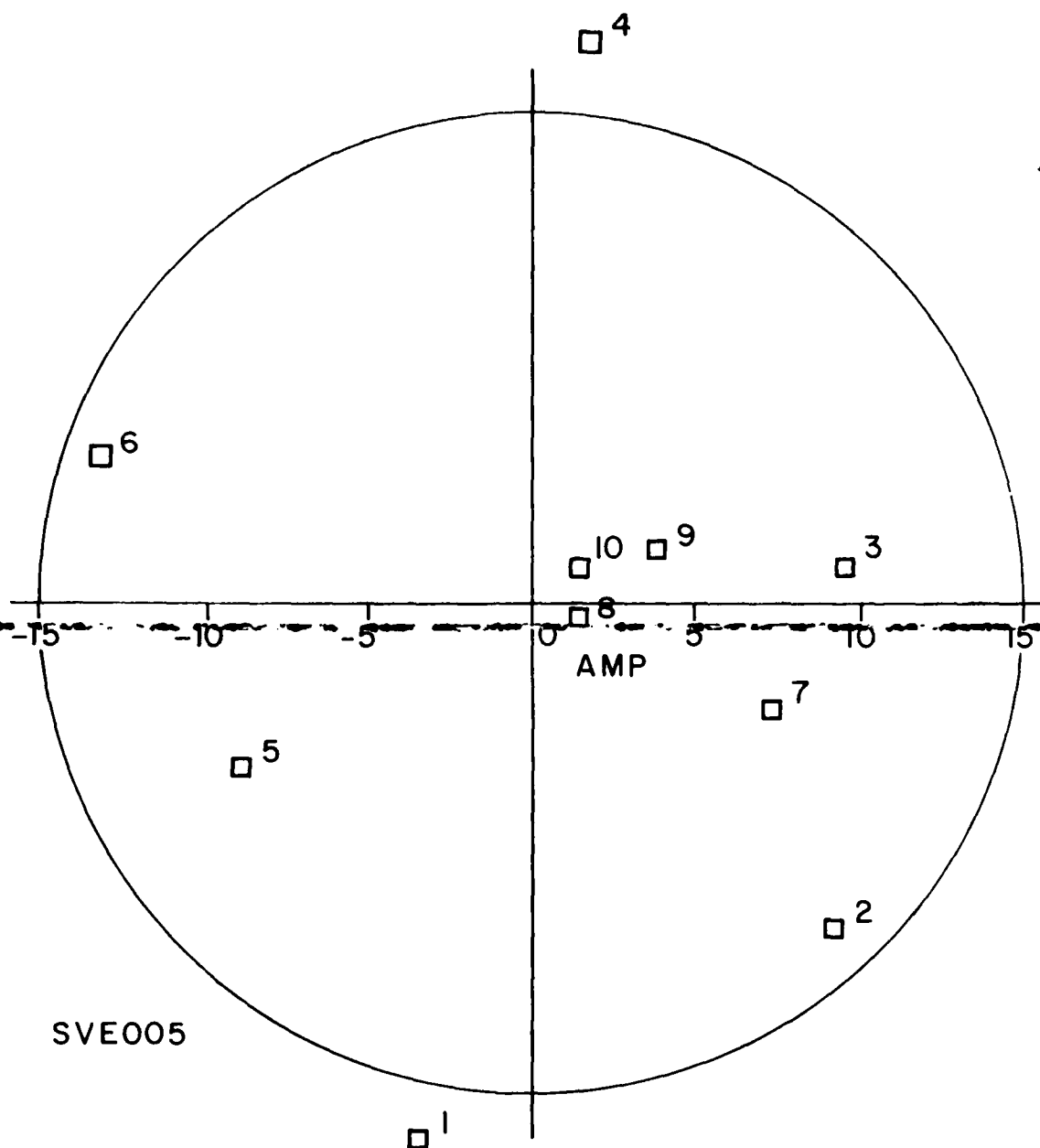Photograph 1 - Models of Missouri and Sverdlov used in this report. (1:700 scale shown)

Figure 1. Example measurement (Sverdlov at 5° off bow). Phasor plot
of the amplitude (square root of the radar cross section -
measured in cm²) and phase of the data for the Sverdlov.
Numbers are the harmonic multiples of 2.17 MHz.

III. NEAREST NEIGHBOR TECHNIQUES

The data from the H.F. radar return of a ship can be represented
by a set of points in a multidimensional space. Each measurement parameter
is represented in a different dimension of the space. Each measurement
at a set of frequencies on a ship will yield a point in this multi-
dimensional space (hyperspace). Measurements at a number of elevation
and aspect angles will yield a set of such points. The behavior of
the set of points determines the overall ability of the radar system to
identify a target. It is necessary for the data processor of the H.F.
radar system to decide which of several candidate groups of points
a new unknown point belongs to.

A number of properties of a set of such points in hyperspace
can be defined. For example, the points for a particular ship may
all lie in a localized region of hyperspace (i.e., they may exhibit
clustering). This would be a useful property. Alternatively, the
points may lie on a line or a surface (actually a hyperline or a hyper-
surface). Conceptually, it is clear that it is not sufficient for
the points measured from a particular ship to cluster in order for
the classification system to be successful. It is also necessary for
the data representing the other ships in the study to occupy some other
location in hyperspace. Nearest neighbor techniques [4] will be used
to study clustering of the ship data in this report, while a hyperline
technique will study the property of separation of the data into distinct
regions of hyperspace.

The technique used to study the clustering property of the data
base available here is called the nearest neighbor technique. This
technique is non-parametric and therefore the statistical properties
of the data need not be known for the results to be valid. The concept
of the nearest neighbor calculation is simple. Each set of measure-
ments of the ship target yields as many as 20 distinct parameters
(i.e., the real and the imaginary parts of the radar cross section

6

at each of the 10 frequencies). This means that each aspect angle
measured for the ship yields a point (or vector) in multidimensional
space and that the space may be defined by as many as 20 dimensions.
The distance between a particular point and each of the other points
in this space may be computed, and the smallest of the distances is
taken as the distance to the nearest neighbor of the original point.
The original point may represent data from an unknown target and the
other points represent data from a set of cataloged measurements of
known targets at various aspect angles and elevation angles. The unknown
point is associated with the target from which the nearest neighbor
was derived. This concept forms the basis for a target classification
algorithm.

In this report, the nearest neighbor technique will be used to
test the clustering property of the data base rather than strictly
as a target identification algorithm. In this way, a more fundamental
property of the original data set may be assessed. The data from a
single frequency scan of a target (the Missouri (1:700) or the Sverdlov
- as mentioned) for a subset of the harmonics available and both with
and without phase data are used to derive a set of points (vectors)
in hyperspace. Then the distance from the point in question to all
of the other points was computed. The minimum of these distances was
used to define the nearest neighbor. For this report, a set of ship
data is clustered if the nearest neighbor to a particular point (or
vector) is a point from the same ship (at some other aspect angle).

An example of the results from this study is given in Table 2.
Abbreviations are used to identify a particular set of data. The
Missouri data measured at an aspect angle of 10^0, for example, is listed
as "MIS010". The left hand column lists the test data (or unknown
data), and the candidate data used for comparison testing is listed
at the top of each column. The numbers are the actual distances which
were computed; they have not been normalized. At the top of the first
column is the first harmonic tested (1) and the last harmonic tested

7

TABLE 2

NN RESULT EXAMPLE

I	II	T	MIS000	MIS005	MIS010	MIS100	MIS175	MIS170	SVE000	SVE005	SVE010	SVE100	SVE175	SVE170
MIS000		0.00E+00	0.92E+03	0.12E+03	0.89E+03	0.85E+03	0.11E+03	0.28E+04	0.25E+04	0.24E+04	0.37E+04	0.21E+04	0.25E+04
MIS005		0.92E+03	0.00E+00	0.87E+03	0.65E+03	0.85E+03	0.67E+03	0.31E+04	0.22E+04	0.27E+04	0.34E+04	0.20E+04	0.23E+04
MIS010		0.12E+03	0.87E+03	0.00E+00	0.88E+03	0.85E+03	0.10E+04	0.27E+04	0.26E+04	0.25E+04	0.30E+04	0.21E+04	0.27E+04
MIS100		0.89E+03	0.65E+03	0.88E+03	0.00E+00	0.31E+03	0.20E+03	0.24E+04	0.19E+04	0.21E+04	0.34E+04	0.21E+04	0.26E+04
MIS175		0.85E+03	0.85E+03	0.85E+03	0.31E+03	0.00E+00	0.19E+03	0.23E+04	0.19E+04	0.20E+04	0.34E+04	0.22E+04	0.25E+04
MIS170		0.11E+04	0.67E+03	0.10E+04	0.20E+03	0.19E+03	0.00E+00	0.25E+04	0.17E+04	0.22E+04	0.33E+04	0.22E+04	0.26E+04
SVE000		0.28E+04	0.31E+04	0.24E+04	0.23E+04	0.25E+04	0.00E+00	0.22E+04	0.50E+03	0.35E+04	0.37E+04	0.29E+04
SVE005		0.25E+04	0.22E+04	0.19E+04	0.19E+04	0.17E+04	0.22E+04	0.00E+00	0.14E+04	0.26E+04	0.31E+04	0.25E+04
SVE010		0.24E+04	0.27E+04	0.25E+04	0.21E+04	0.20E+04	0.22E+04	0.14E+04	0.00E+00	0.28E+04	0.30E+04	0.22E+04
SVE100		0.37E+04	0.34E+04	0.38E+04	0.34E+04	0.33E+04	0.35E+04	0.26E+04	0.28E+04	0.00E+00	0.29E+04	0.67E+03
SVE175		0.21E+04	0.20E+04	0.21E+04	0.21E+04	0.22E+04	0.22E+04	0.31E+04	0.30E+04	0.29E+04	0.00E+00	0.22E+04
SVE170		0.25E+04	0.23E+04	0.27E+04	0.26E+04	0.25E+04	0.29E+04	0.25E+04	0.22E+04	0.67E+03	0.22E+04	0.00E+00

(10). The T indicates that phase measurements were used to convert
the data to real and imaginary components prior to computing the neighbor
distances. There were a total of 20 dimensions used in the example
shown. The example shown has had the nearest neighbor value (minimum)
underlined. If the nearest neighbor is in fact, the other ship, the
value is underlined twice. The entire set of nearest neighbor results
is given in Appendix B. The data given in Appendix B (and in Table 2)
give all distances in multidimensional space between the test target
and the catalogued data - no normalization has been used. A total
view of the clustering properties of the data base can be found in
this appendix. Some of the general behavior of the nearest neighbor
calculations for all the data can be seen in the example shown in Table
2. It can be seen that the nearest neighbor is typically not only
from the same ship as the test (unknown) data, but is also close in
aspect angle to the test data.

Note that the comparisons between identical data sets will always
produce a zero value in this noiseless or errorless type of study.
If the statistics of the errors can be defined in a meaningful way,
then artificially introduced signal corruption could be included in
the study and a measure of the expected performance of the nearest
neighbor algorithm for target identification could be studied. This
type of study will be included in future research tasks.

The example shown here has an anomalous point. The nearest neighbor
of the Sverdlov at 175° aspect angle (SVE175) is a data point for the
Missouri at 5° aspect angle (MIS005). Note however, that the nearest
neighbor in this case is not very near. In fact, the nearest neighbor
distance for SVE175 is more than an order of magnitude larger than
several of the other nearest neighbor distances. Note (assuming the
data base is accurate here) that this error does not mean that the
nearest neighbor test for target identification would necessarily fail
in this case. It is likely in practice that the catalog of data would
contain measurements of the Sverdlov at 175° for comparison with an

9

unknown target which would also be the Sverdlov at 175° in this case. Only
the errors in the measurements would contribute to misclassification.
On the other hand, if the data base is valid, this test has identified
a sensitive area for further study. It can be seen that small changes
in the aspect angle have introduced large changes in the features
of the H.F. radar return, namely the data are not clustered at this
aspect angle.

A summary of the nearest neighbor tests is given in Table 3.

TABLE 3

NN SUMMARY

NEAREST NEIGHBOR

| HARMONICS | BROADSIDE | | | BOW-STERN | | |
| | ALL ASPECTS | | AMP +/-5° | ALL ASPECTS | | AMP +/-5° |
	AMP P:Q	AMP+Ph P:Q	P:Q	AMP P:Q	AMP+Ph P:Q	P:Q
1-5	9:10	7:10	9:10	12:12	12:12	12:12
3-7	9:10	9:10	10:10	12:12	10:12	12:12
6-10	6:10	8:10	5:10	12:12	11:12	12:12
1-10	5:10	7:10	6:10	12:12	11:12	12:12

P = Number of times that the nearest neighbor of a target
was the same target but at a different aspect angle.

Q = Number of cases.

P ÷ Q is a measure of the "clustering" property of the data.

Ties counted as clustered.

CONCLUSIONS:

   The BOW-STERN data are all well clustered. Identification
   should be possible even with large measurement errors.

   The lower order harmonics exhibit more clustering than the
   higher order for the broadside data.

10

In this table, the data were grouped in various subsets of the total number of available harmonics. The ratio of clustered points (P) to the number of comparisons (Q) is given in this table. The first three entries in the table all use 5 harmonics. This represents 5 dimensions for the amplitude only cases and 10 dimensions for the amplitude and phase (real and imaginary components) cases. Note that all of the bow-stern amplitude only cases are well clustered (i.e., 12:12). A test of data comparisons using only $+/-5^{o}$ aspect angles is also presented in this table. This is a test of the clustering of the data if a priori information on the aspect angle is available. It is possible to see that poor clustering is not caused by including too many aspect angles in the test data. It can also be seen that the clustering of the broad-side data is not improved by the introduction of phase data into the algorithm. In fact, in some cases, the clustering is degraded by the introduction of phase information. Finally, note that the data from the lower order harmonics exhibit more clustering than the higher order harmonic data.

It should be emphasized that degradation of the clustering property of a set of data does not mean that the identification potential of the data has been reduced. It may, in fact, have been increased since less clustering means the data are more spread out in feature (multi-dimensional) space and thus less sensitive to noise, clutter, etc. On the other hand, reduced clustering as defined in this report does mean that the aspect angle sensitivity has been increased (as might be expected for higher harmonic numbers or the introduction of phase). Thus the catalog of measurements required for identification of a particular target must include a larger set of aspect (and elevation) angles if the clustering is reduced.

In conclusion, then, the data are well clustered for the bow-stern group, and for the lower order harmonic values at broadside. A priori information does not increase the clustering, and neither does the introduction of phase information. These general results

11

are expected to be applicable to the full scale OTH measurements taken
by the NRL SEA ECHO system. In other words, it is expected that ampli-
tude data alone on full scale ships will cluster well for bow-stern
and will probably cluster somewhat at broadside aspect.

IV. HYPERLINE STUDIES

It is not sufficient for data in multidimensional space to cluster
in order to be able to confidently predict the identifiability of the
ship targets using H.F. radar return information. The clusters must
also separate from each other by an amount greater than the expected
measurement errors. Algorithms for exploiting the data for target
identification may then be confidently developed and tested. Furthermore,
clustering is not the only property that predicts the identifiability
of the ship targets in the data base. It can be shown, for example,
that the data points in multidimensional space derived in the study
in this report should form closed curves. This may be seen if it is
noted that the only variable in the data base presently in use is the
aspect angle. The only geometric configuration that results from a
function with a single independent variable (modulo 2π) is a closed
curve. This curve may be quite complex, of course, but this complexity
is constrained by the observation from the data base used here that
there is a reasonably smooth progression in the backscatter data as
the aspect angle is changed. There are also theoretical limits to
the complexity of these closed curves. These are related to the size
of the ships in proportion to the wavelength at H.F. (See the section
on time domain studies.)

The study undertaken to quantify these ideas was taken from a
representation of the data as points (or vectors) in a multidimensional
space. The curves which result from a variation in aspect angle for
the two targets will be separated from each other by some distance,
D. This distance may be computed for the given data over restricted
ranges of aspect angles. The method is illustrated by Figure 2. It
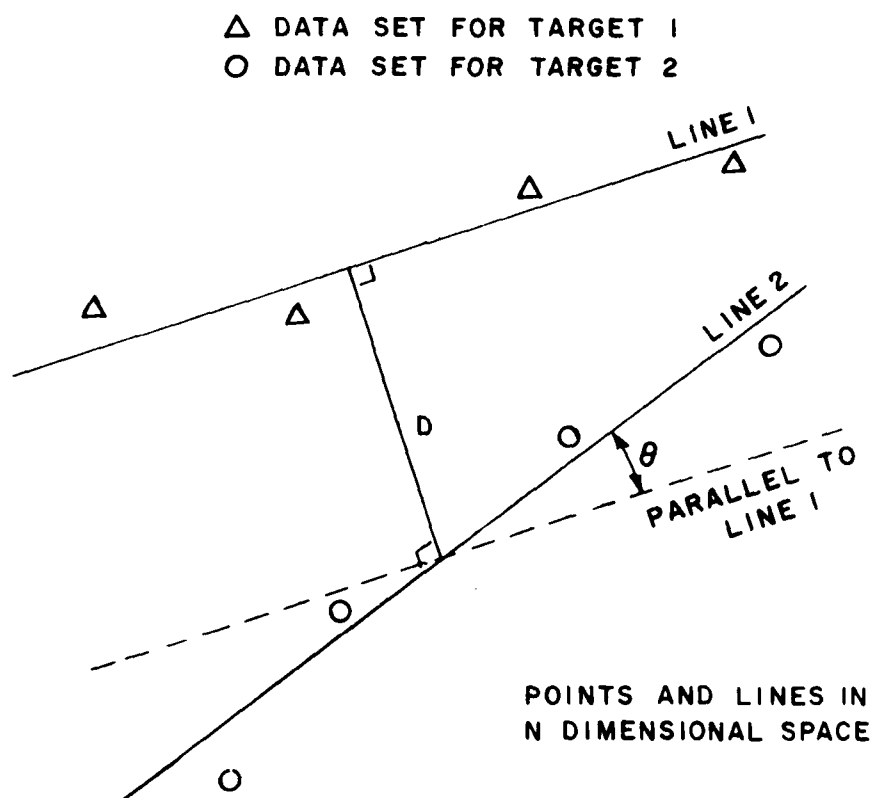is summarized below.

12

Figure 2. Hyperline concept - definitions of D and θ.

(1)   Restrict the range of aspect angles (and number of harmonics).

(2)   Fit a straight line to each set of points over the range of aspect
       angles chosen. (The "goodness of fit" of the set of points to
       a straight line will determine the applicability of the data
       to this type of treatment.)

(3)   Compute the distance D between the two straight lines in multi-
       dimensional space (hyperlines) at their closest approach, and
       the skew angle, θ, between the two hyperlines. The computations
       used and the derivation of the equations are given in Appendix
       C.

This procedure reduces the description of the separation of two
multiparameter feature sets to a scalar number D. The value of D can
be computed as a function of the number of frequencies used and the
range of aspect angles chosen. The parameter θ is a measure of the
skewness of the two hyperlines. This parameter gives a measure of
the sensitivity of the distance D to changes in aspect angle. If the
value of θ is near 0° or 180°, then the two lines are nearly parallel,
and the distance between them will remain unchanged for relatively
large changes in the aspect angle. If the value of θ is near $\pm 90^{\circ}$
(right angles) then, the two lines are crossing each other, and relatively
small variations in aspect angle will result in larger values of D.
Thus radar data which has values of θ near $\pm 90^{\circ}$ will have better sta-
tistical properties for target identification than radar data with
values of θ near 0° or 180°.

The data used in the nearest neighbor example (Missouri (1:700
and Sverdlov) was also used to compute D and θ for groups of harmonics
over limited aspect angle ranges as shown in Table 4. In this table,
groups of 4 harmonics were used over aspect angle scans of the broad-
side, bow and stern. As can be seen, this table indicates that the
best frequency range (largest value of D) occurs for harmonics 4 through

14

TABLE 4
D AND θ FOR MISSOURI AND SVERDLOV
VS. FREQUENCY BAND

Dist. (min.) and Skew Angle in Hyperspace.
Missouri Versus Sverdlov

ASPECT ANGLES
$80^{\circ} - 85^{\circ} - 90^{\circ} - 95^{\circ} - 100^{\circ}$

HARMONICS	DIST.	ANGLE(deg)
1 - 4	10.3	116
2 - 5	14.9	111
3 - 6	12.1	35
* 4 - 7	16.0	68
5 - 8	15.9	59
6 - 9	13.1	64
7 - 10	14.6	85

ASPECT ANGLES
$170^{\circ} - 175^{\circ} - 180^{\circ}$

HARMONICS	DIST.	ANGLE(deg)
1 - 4	19.1	143
* 2 - 5	28.2	30
3 - 6	12.0	64
4 - 7	24.6	39
* 5 - 8	28.2	28
6 - 9	14.1	127
7 - 10	21.8	124

ASPECT ANGLES
$0^{\circ} - 5^{\circ} - 10^{\circ}$

HARMONICS	DIST.	ANGLE(deg)
1 - 4	49.8	120
2 - 5	59.9	129
3 - 6	48.8	103
4 - 7	23.0	68
5 - 8	59.7	95
* 6 - 9	62.1	149
7 - 10	53.2	105

7 at broadside, harmonics 6 through 9 at bow on, and for harmonics
2 through 5 or 5 through 8 (a tie) for the stern view. These harmonics
are preferred with more than a two to one margin for the bow or stern
aspects. The broadside aspect choice of frequency range is less clear
if only the value of D is considered. If the value of theta is included
in the argument, however, the choice of the 4 to 7 harmonic range for
optimum target identification is strongly indicated. The choice of
frequency range for the stern aspect is complicated by the introduction
of θ. In this case, large values of D are accompanied by values of θ
which are less desirable (i.e., close to 0°).

An important use of this computation would be in the compari-
son of the value of D to the expected measurement errors. If D is
significantly larger than the expected measurement errors, then the
data from the OTH radar return from ships as studied here would be in-
herently useful for ship identification. Since the error statistics
of radar cross section measurements by full scale systems is not yet
available, this comparison is not yet possible. A comparison with
the average magnitude of the backscatter return is possible, however.
The results are given below for the values used in Table 4.

<div style="text-align:center">

broadside D = 16.0, Amp (typical) = 40.

ratio = 0.4

stern D = 28.2 AMP (typical = 10

ratio = 2.82

bow D = 62.1, Amp (typical) = 10

ratio = 6.21

</div>

These results are very encouraging. The implication is that errors
on the order of 3 (stern) or 6 (bow) times the typical backscatter
measurement level can be tolerated and the data sets will still be
separated in terms of the features available for identification. The

broadside results indicate that the cross section must be measured within 40% of the value of a typical magnitude in order to insure feature set separation. The magnitudes, on the other hand, will be larger and the absolute measurement accuracy required at broadside may be the same as at bow or stern aspects. These results will be discussed further in the last section of this report.

V. TIME DOMAIN FEATURES

This section discusses the application of Transient Electromagnetic Signature research to the problem of identifying distant ships and aircraft from Over-the-Horizon (OTH) Radar returns. First, the signature quantities are defined, and some past research on the signatures, their nature and their utilization is discussed. Next recommended requirements for data collection based on the nature of target transient signatures are discussed. Then two important approaches to ship identification are described assuming that the necessary OTH data are available. The first approach involves the information contained in the initial portion of the transient echo return waveform, and infers geometrical quantities of the body. The second approach involves the latter portion of the time-domain signature and relates to the characteristic resonances of the object. A final section briefly reviews the application of these approaches to over-the-horizon aircraft identification.

The use of the transient radar signature of object was first discussed by Kennaugh and Cosgriff in 1957 [5]. Since then, considerable research effort has been done concerning basic transient signature properties [6], calculation of transient signatures for specific bodies [7], and antennas for possible transient radar use [8]. The time-domain transient signature used in this effort is the ramp response waveform, which was first suggested for radar identification by Kennaugh and Moffatt [6]. This signature is defined as the far-zone backscattered time domain waveform of a target illuminated by a traveling planar transverse electromagnetic field unit slope discontinuity. The impulse, step, and ramp response signatures of a sphere are shown in Figure 3.
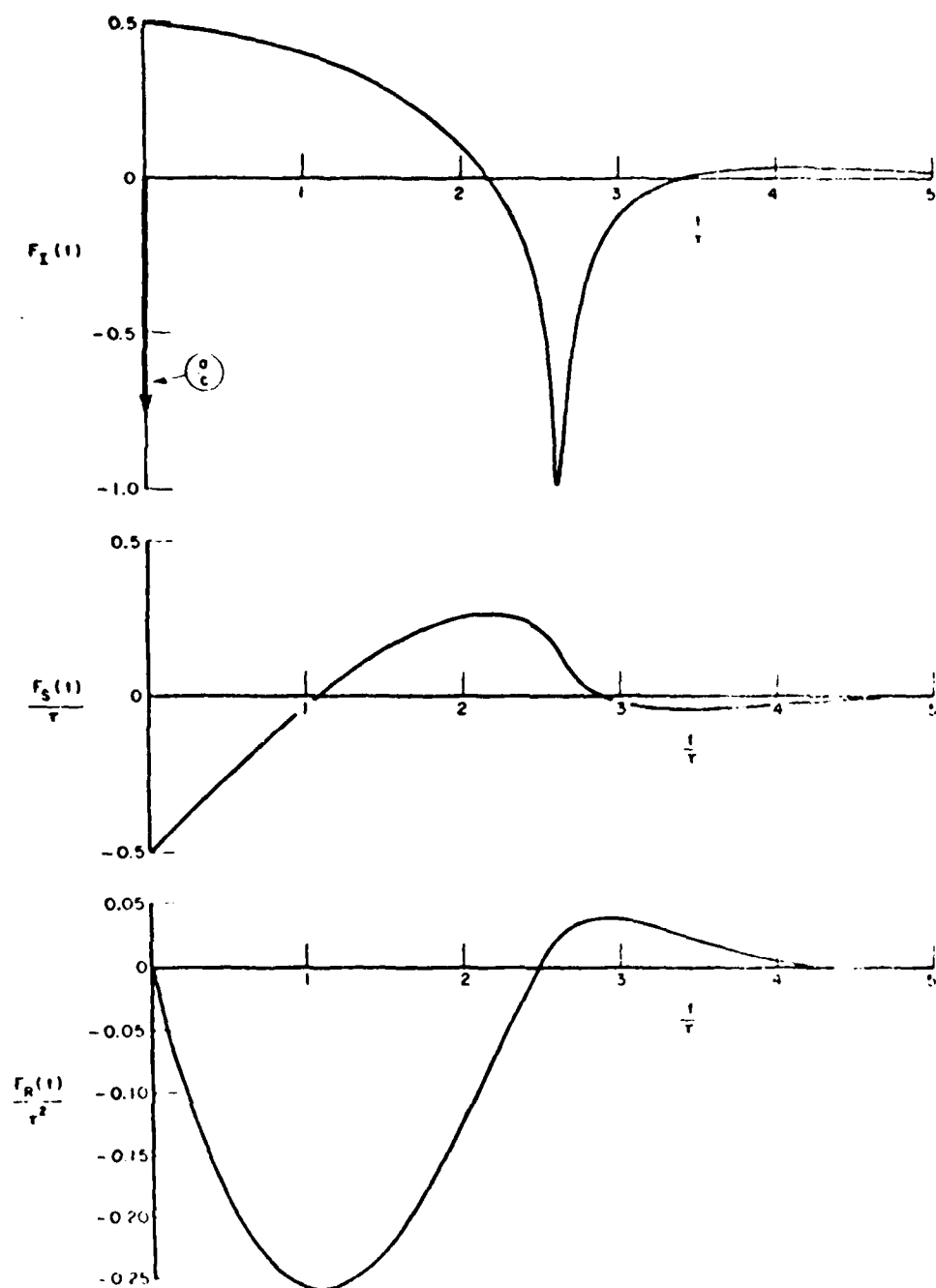
17

Figure 3. Characteristic backscattered waveforms
of a conducting sphere.

18

The ramp response signature is the *second integral* of the impulse response of a target, and hence shares several of its useful properties. The ramp response is unique with respect to target shape, orientation, and material composition. It is the *inverse Fourier transform* of a target's complex backscattering frequency spectrum multiplied by the factor $(1/(j\omega))^2$:

$$R(t) \qquad (\frac{1}{j\omega})^2 \sqrt{\sigma(\omega)}. \qquad (1)$$

Because of the $(1/(j\omega))^2$ factor, Kennaugh and Moffatt predicted that satisfactory approximate ramp response signatures could be obtained with narrower bandwidth interrogating signals than for the impulse response. For example, ten-harmonic approximations of the sphere impulse and ramp response waveforms are shown in Figure 4. The fundamental frequency has wavelength approximately five times the sphere diameter. As can be seen, the major features of the ramp response waveform are faithfully reproduced.

It should be noted that these signatures are all functions of aspect angle and polarization of the interrogating signal with respect to the target. Thus, quantitatively

$$\frac{G(\rho,\theta,\phi,j\omega)}{(j\omega)^2} = \int_0^\infty R(\rho,\theta,\phi,t)e^{-j\omega t}\,dt$$

where

$$\pi c^2 |G(\rho,\theta,\phi,j\omega)| \equiv \sigma(\rho,\theta,\phi,j\omega)$$

and ρ,θ,ϕ emphasize the dependence on polarization and interrogating signal direction.
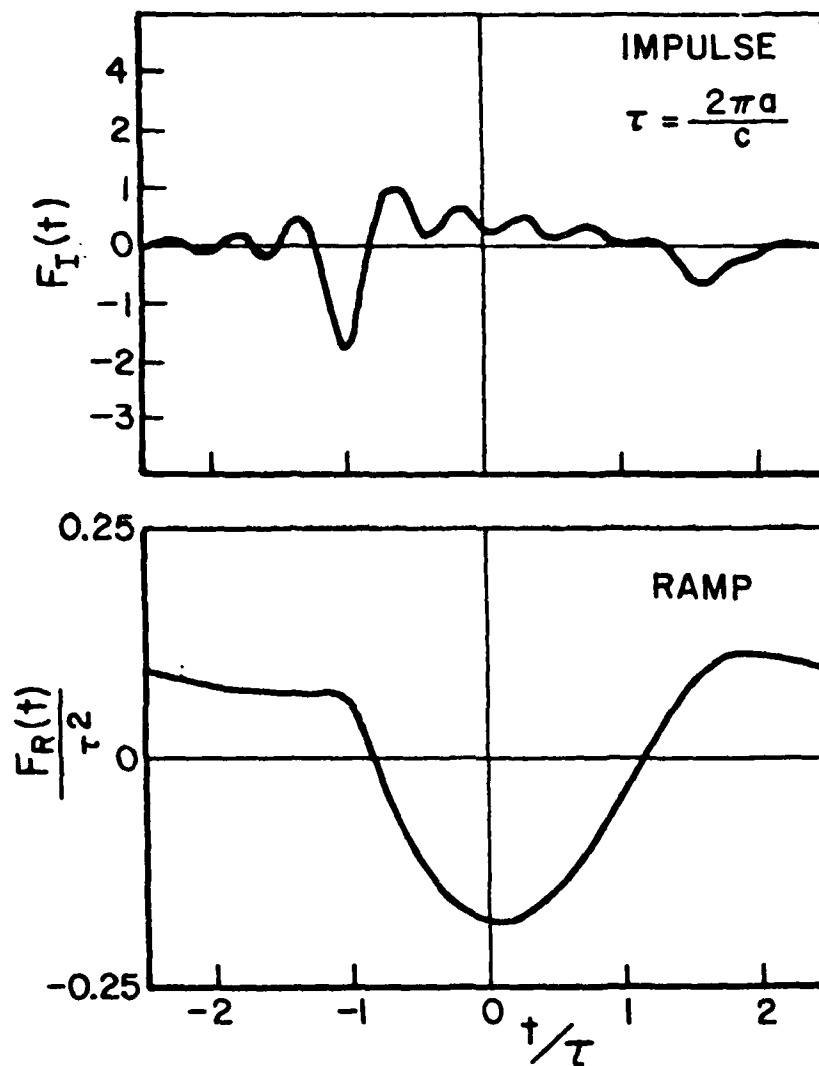
Figure 4.   Ten-harmonic approximate sphere transient signatures.

20

Data Requirements for Generating
Ramp Response Signatures

Because of the Fourier Transform relationship it is obvious that
signature data may be gathered either by the use of time-domain transient
interrogating radar signals, or by measuring the complex backscattered
cross-section of a target at sampled frequencies in the frequency domain.
As was already shown, adequate ramp response signatures for simple
shapes are obtained from data at as few as 10 harmonically related
frequencies.

Based on known ramp response characteristics, we can calculate
the frequency sampling interval for valid signature reconstruction,
and the relative importance of the different frequencies. First, it
is known that the ramp response signature is of finite duration. Using
a conservative estimate based on past measurements, the duration of
the signature is less than 6 transit times across the length of the
object, i.e.,

$$R(\rho,\theta,\phi,t-t_0) = \begin{cases} 0 \ (t-t_0) < 0 \\ 0 \ (t-t_0) > \dfrac{6\ell}{c} \end{cases}$$

where this ramp response in retarded time begins at time t_0, ℓ equals
object length, and c is the speed of light.

For a time-limited function, application of the Shannon sampling
theorem produces a required frequency sampling interval. Specifically,
given

$$f(t) = 0 \text{ for } |t| \geq T,$$

then

$$F(\omega) = \sum_{n=-\infty}^{\infty} F(\frac{\pi n}{T}) \frac{\sin(\omega T - n\pi)}{\omega T - n\pi} \quad .$$

21

Thus, for a given object length ℓ, the scattering signature of the object should be sampled at intervals of

$$f_n = \frac{\pi n}{T(2\pi)} \qquad \text{and } T = \frac{1}{2}\left(\frac{6\ell}{c}\right) ;$$

$$v_n = \frac{nc}{6\ell} = \frac{n \times 3\times 10^8 \text{ meters/sec}}{6 \; \ell_{\text{meters}}} .$$

This formula implies that for an aircraft carrier of 300 meters length, the sampling frequency interval should be 183 KHz. For a destroyer of 125 meters length, a sampling frequency interval of 400 KHz or less is sufficient. It should be stressed that these numbers are derived from worst-case signature characteristics and are sufficient for all cases. For some aspects and interrogating polarizations, sampling this often in frequency may not be necessary. On the other hand, maintaining such sampling intervals in these cases provides some redundant information, in effect improving the signal to clutter performance of the signature measurement system.

Another important feature of the ramp response signature is its $|1/\omega^2|$ weighting of frequency domain cross-section data. This weighting emphasizes the low-frequency scattering characteristics of targets. For example, it means that acceptable ramp response signatures may be derived from frequencies below 12 MHz for all ships larger than 125 meters long.

Target Geometry vs. Ramp Response Signature

One of the most attractive features of using ramp response signatures derived from over-the-horizon radar is that the first portion of the ramp response approximates the target "profile function" for metallic targets [9]. A calibrated ramp response, containing both amplitude and phase vs. frequency input, is approximately equal to the target cross-sectional area vs. distance along the line of sight.

22

Thus, particularly for near-bow and near-stern look angles, it is seen that such a signature carries considerable information on the gross features of a ship.

The above relationship has been demonstrated using measured data for simple shapes like cones, cylinders, spheroids etc. [9,10]. It was examined for ship targets on this program, using the measured model scattering data (Table 1).

The size of all the measured ship models were too large for the frequency sampling criterion just discussed to be satisfied. Therefore, aliasing is present in all of the reconstructed ramp response waveforms. The smallest ship models were chosen for study, because it was expected that their data would be most accurate. The amplitude spectra for these two ships for nose-on incidence are shown in Figure 5 (Hayanami) and Figure 6 (Shimokaze) [3]. It is very interesting to note that, despite the fact that the two destroyer models are almost of identical size and have many similarities in their gross structural outlines, there is a relative null feature in the Hayanami spectrum which does not appear in the Shimokaze spectrum. There is not a data point to define the actual depth of this null which was generated by the spectrum smoothing process. However, some features of the ramp responses tend to confirm its existence and explain why it happens.

The approximate ramp response waveforms for these ships are shown in Figure 7, along with correctly scaled profile outlines of the two ships. It is noted that there appears to be experimental model position-ing error in the nose-on look angle measurement of the Shimokaze. It should probably be moved ≃ 3 cm forward to agree with the stern look angle waveform.

There is an important difference in the waveforms of these two ships, which probably explains the relative null. It is seen that the Hayanami has two peaks, corresponding to the forward and aft vertical
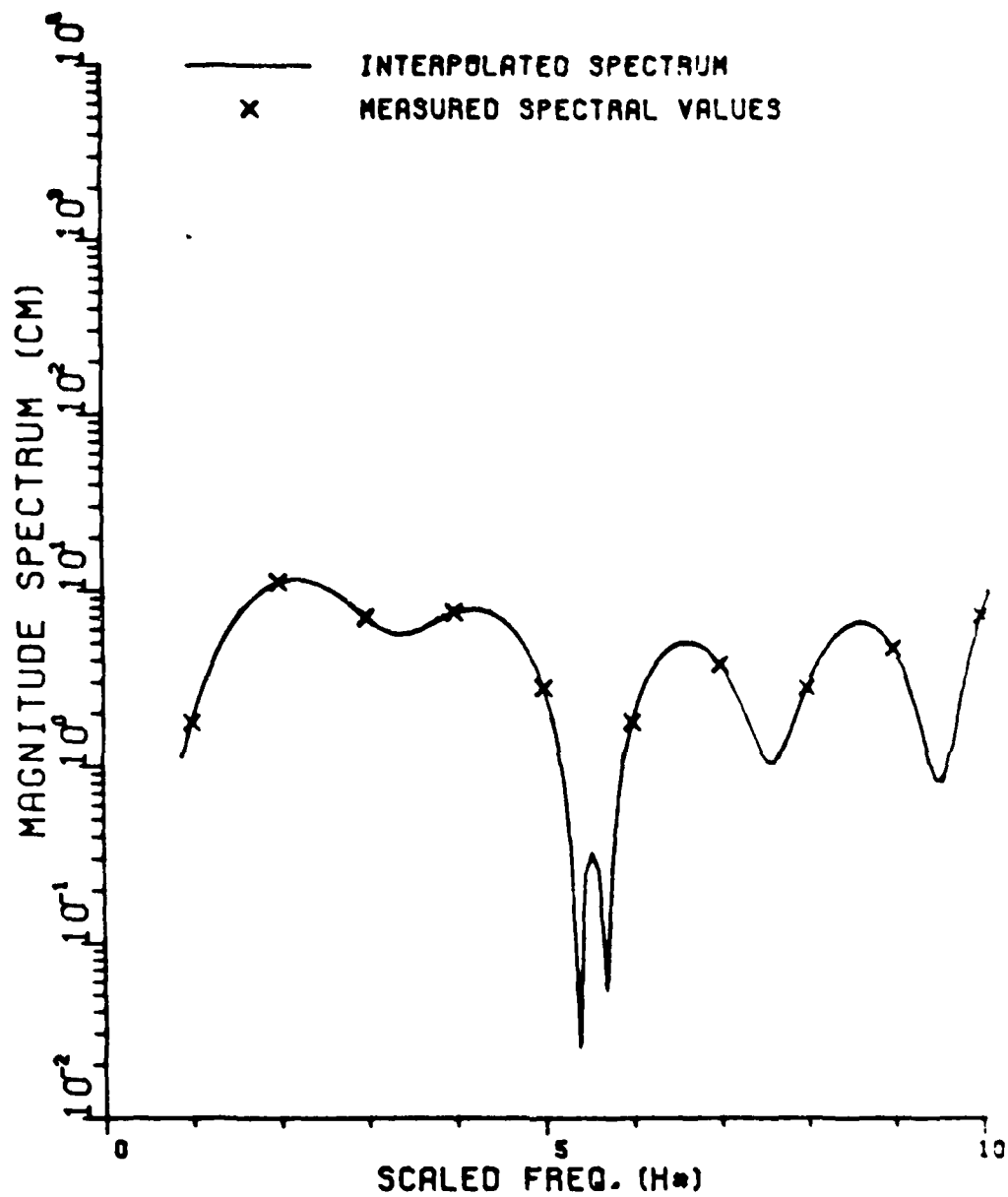
Figure 5.   Magnitude spectrum vs. scaled frequency for the
Hayanami (1:700) - bow on.

24
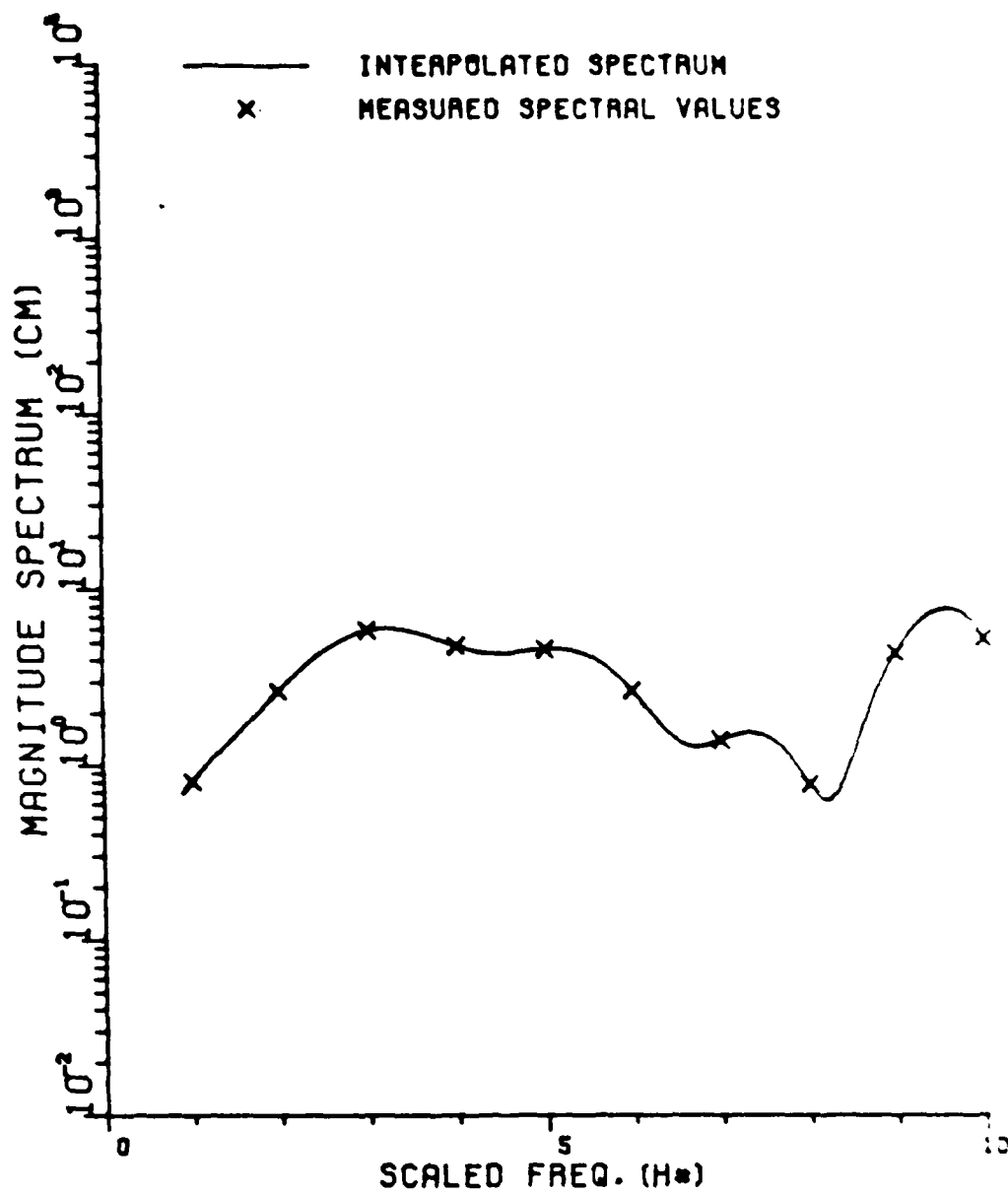
Figure 6. Magnitude spectrum vs. scaled frequency for the Shimokaze (1:700) - bow on.
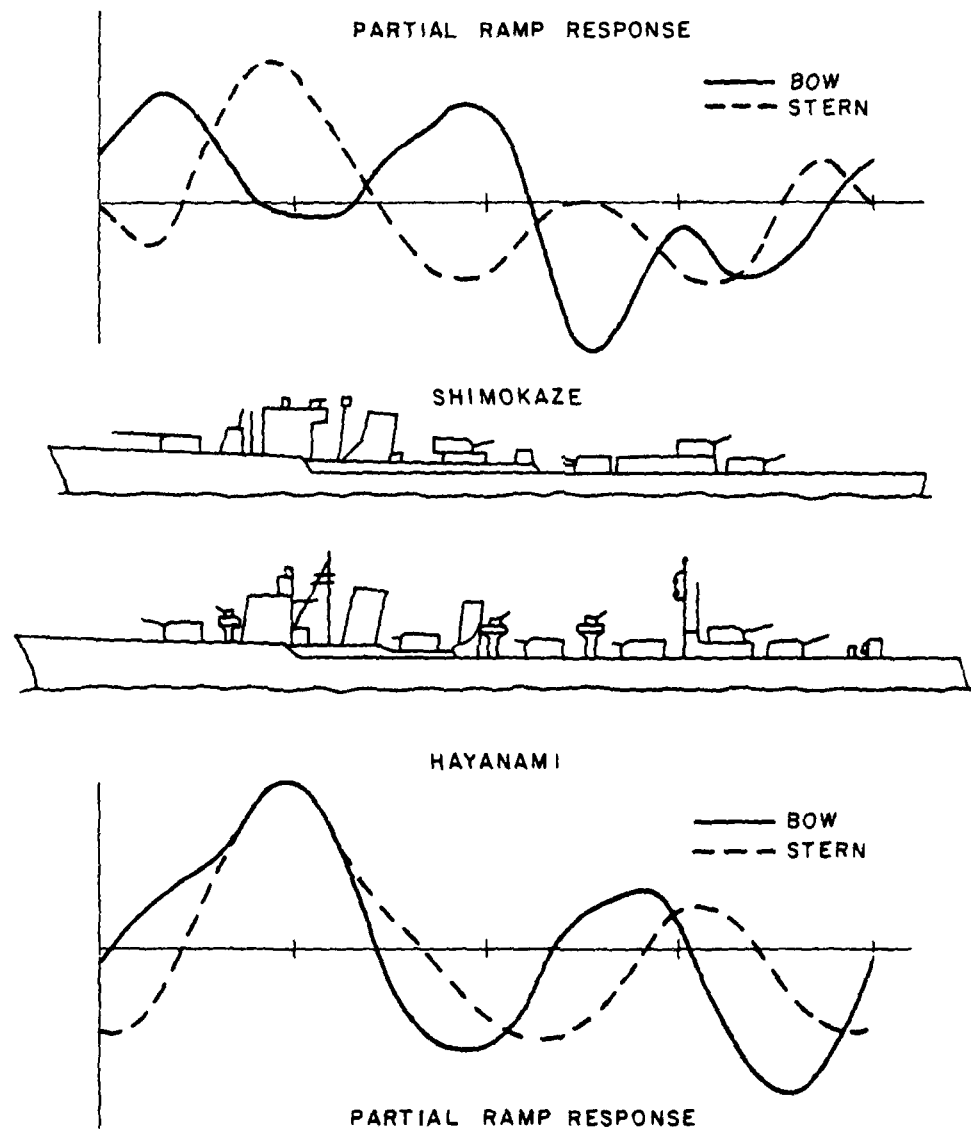
Figure 7. Ramp response results and ship outlines.

26

masts. The relative null in the Hayanami frequency sepctrum simply reflects an interference effect between the approximately equal strength echos of the fore and aft masts. The Shimokaze does not have an aft mast structure, and hence has only one major peak in its ramp response.

Two conclusions are drawn from this information. First, the measured ramp response data shows promise as a tool for determining which structures on the ship make major contributions to the scattering signature vs. frequency, time-delay, and aspect angle. Thus, even though it is probably impractical to reconstruct a ramp response signature with an operational system, it would be important to perform further ramp response research on models in order to guide a selection of re-liable, geometrically meaningful features in the frequency domain for the operational system. A second conclusion is that for these two ships, the scattering at near on-axis look angles primarily reflects the vertical masts.

VI.   SHIP TARGET CHARACTERISTIC RESONANCES

Concerning the complete transient response (impulse, step, or ramp) of a ship, the time domain waveform contains the initial profile function just discussed followed by a decaying complex exponential portion which is characterized by the natural resonances of the object. It is important to note that while the amplitudes and phase of their excitations may change as a function of direction and polarization, the poles in the complex plane which correspond to the natural resonances are invariant.

Two theoretical and experimental efforts using natural resonances for target identification have been studied and evaluated for potential application to OTH radar returns. The first effort involved transient radar measurements of buried metallic and non-metallic targets [11]. The second effort is the one whose model measurement data has been used in this report, concentrating on radar frequencies of 1.42, 2.84 ... 14.2 MHz incident on ships.

The underground radar study dealt with metallic and non-metallic objects, few of which were strongly resonant. A target set is shown in Figure 8, and a set of poles obtained from measured data is shown in Figure 9 for one target. These data show that for the first few poles, their location is almost excitation invariant. It is also important that for these targets which are not strongly resonant, the poles can be extracted from measured scattering data.

Poles have also been extracted for the ship models [3], although their locations seem to be somewhat dependent on ship orientation. There are two possible reasons for this: 1) The data have aliasing, and 2) the ship models are more complex, and therefore should have more natural resonances than the simple underground targets.

Techniques have been devised for target identification using target poles. It is found that identification requires only a portion of the total excitation spectrum, and is independent of target aspect angle. Based upon these features, the characteristic resonances of ships are regarded as promising candidates for use as features for identification using OTH data. These resonances need to be studied further, with a data base that is not degraded by aliasing.

Finally, previous studies have shown that transient signatures are a useful tool for guiding the selection of features for aircraft identification. In particular, identification techniques using frequencies pertinent to OTH radar have already been developed [12].

VII. CONCLUSIONS AND OVERVIEW

A number of studies have been performed with the goal of developing a system for the automatic identification of ships using the radar return from an H.F. over the horizon (OTH) radar system. This phase of the research has been involved with using available techniques and an available data base to study the general identifiability of ships

28

30.5 cm

12.7 cm

PLASTIC MINE-LIKE TARGET

30.5 cm

10.2 cm

(0.5 cm WALL THICKNESS)

BRASS CYLINDER

14.6 cm

ALUMINUM SPHERE

20 cm

←20 cm→

COPPER SHEET

5.1 cm

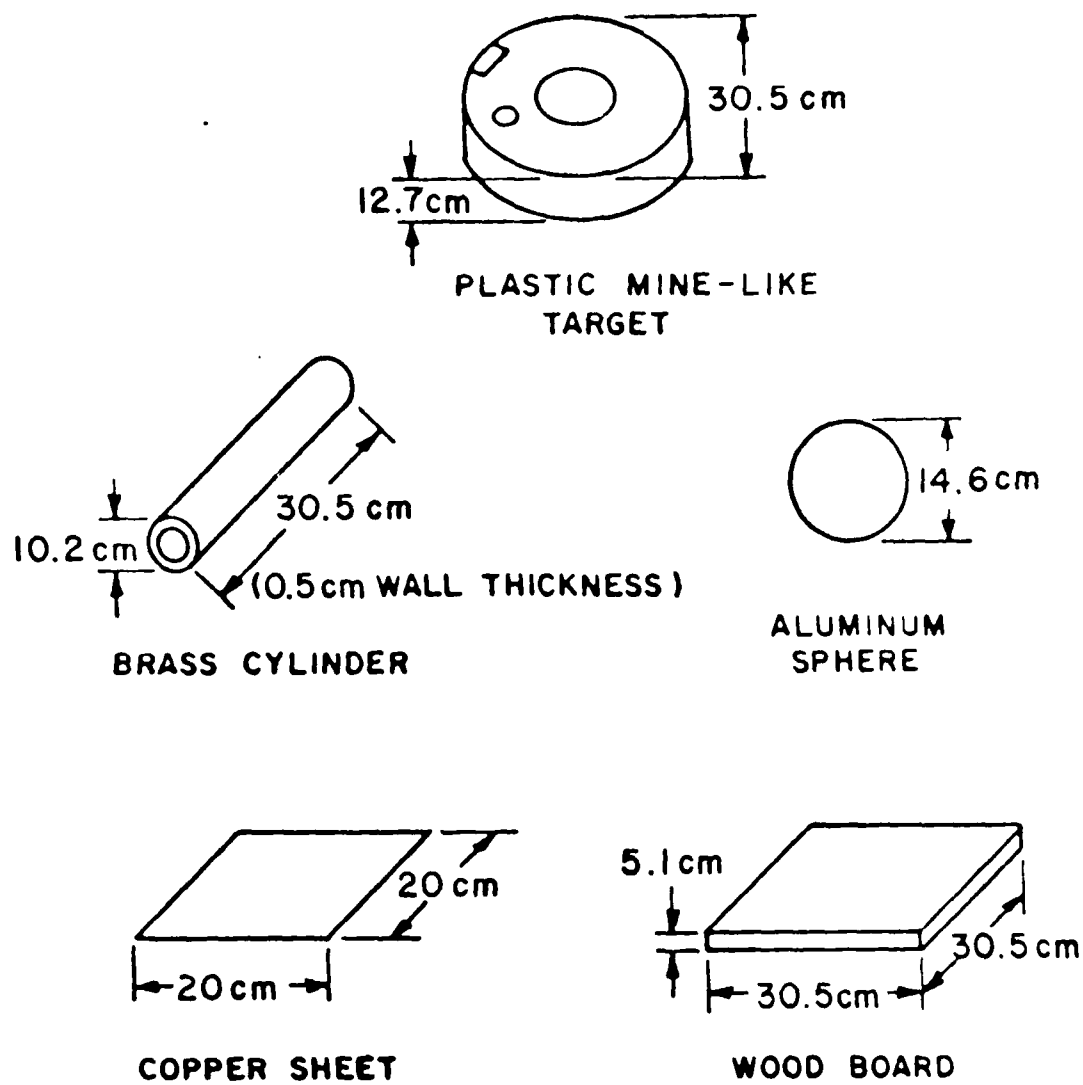30.5 cm

←30.5 cm→

WOOD BOARD

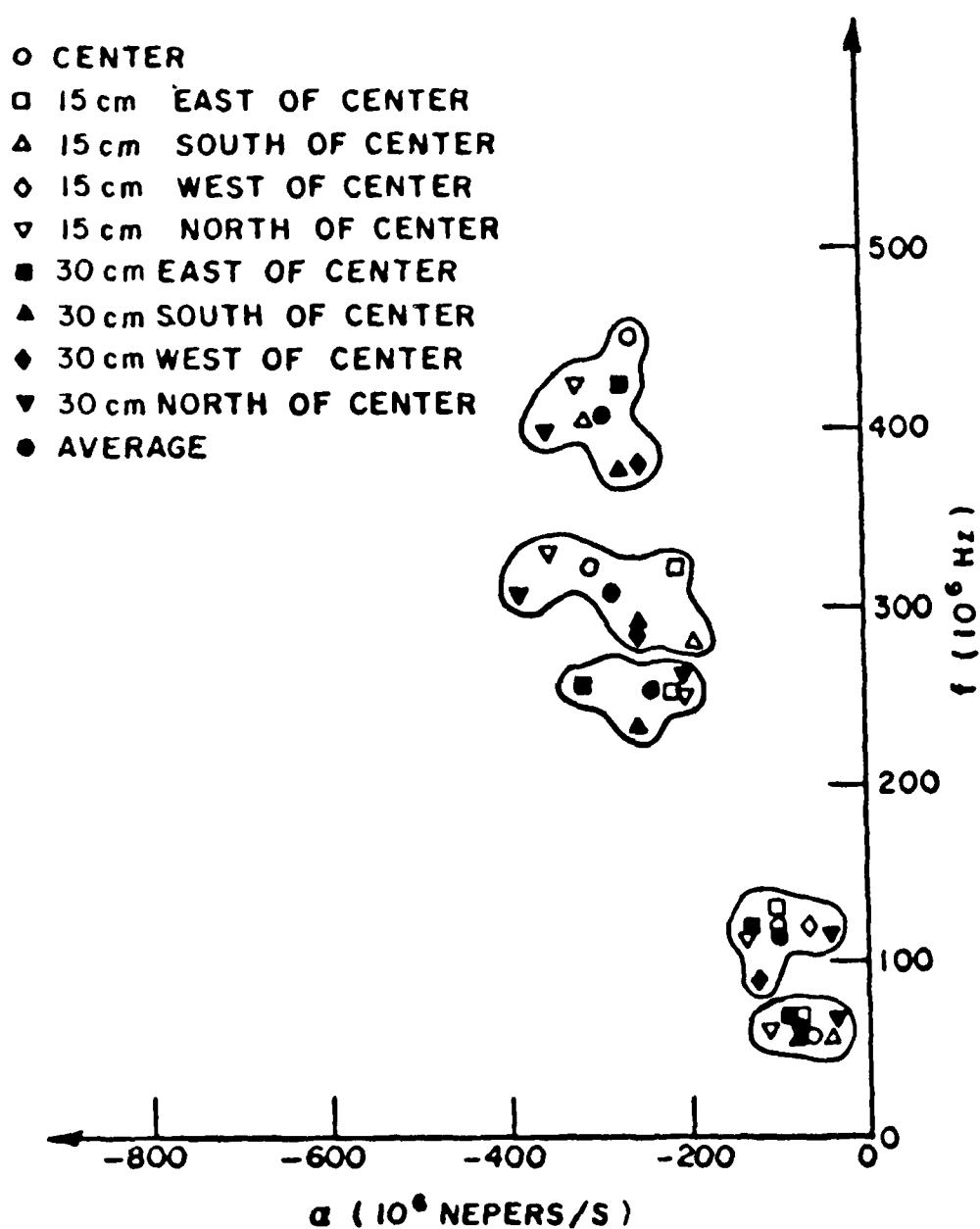Figure 8.   Physical characteristics of the subsurface targets.

Figure 9. Location of the extracted resonances of the mine-like target at different antenna locations in icy ground.

based on OTH radar returns. The results are quite encouraging. It has been shown that in general, ships are inherently identifiable from H.F. OTH radar data. The features cluster and separate far enough to accommodate large error margins. This means that the application of specific pattern recognition techniques to this problem can be expected to yield good results. The choice of the particular algorithms to employ for automatic target identification will depend on further studies of data and of the error mechanisms and statistics found in operational OTH systems.

Studies in the time domain complement these results. These studies have shown that the large significant structures on a ship are the major contributors to the H.F. radar return. Quantitative values of the sampling density in the frequency domain were derived using time domain techniques.

The frequency domain and the time domain results are also in agreement with regard to the aspect angles which are important for future study. Both techniques indicate that broadside data from a ship is most difficult to use for target identification. One reason suggested for this is that the broadside data are stronger than the bow data because of the large return from the hull of the ship. Since the identification characteristics have been shown to be related to the arrangement of the superstructure, the return from the hull of the ship at broadside can be thought of as a clutter contribution. This "clutter term" is large at broadside, but small at bow and stern aspects. The return from the superstructure, on the other hand, is of the same order of magnitude for the bow and broadside cases. Studies in this area should be continued.

Future studies of H.F. OTH radar identification of ships have a prerequisite for a specialized data base. The data base should be designed for ship target identification using data from H.F. radar. This means that a set of data for full aspect angle coverage and 0^0

31

to 30° elevation angle coverage for a number of ships should be obtained.
The frequency coverage should be consistent with the constraints mentioned
in Section V of this report. The ships to be studied should be chosen
based on the need to support a full scale OTH H.F. radar system. This
data base should be of sufficient quantity to allow development and
testing of the performance of target identification algorithms relevant
to the full scale operational system. Comparisons between the model
measurements and the full scale measurements will be made. Testing
of target identification algorithms on the available full scale measure-
ments can then begin.

REFERENCES

1. J. D. Young, R. A. Day, F. B. Gross and E. K. Walton, "Basic Research in Three-Dimensional Imaging from Transient Radar Scattering Signatures," Report 784785-1, July 1978, The Ohio State University ElectroScience Laboratory, Department of Electrical Engineering; prepared under Contract DASG60-77-C-0133 for Ballistic Milliles Defense Systems Command, Huntsville, Alabama.

2. D. L. Moffatt and C. M. Rhoads, "Radar Identification of Naval Vessels," Report 784558-1, December 1977, The Ohio State University ElectroScience Laboratory, Department of Electrical Engineering; prepared under Contract N00014-76-C-1079 for Department of the Navy, Office of Naval Research, Arlington, Virginia.

3. C. M. Rhoads, "The Identification of Naval Vessels via an Active Multifrequency Radar System," Masters Thesis, The Ohio State University, 1978.

4. R. O. Duda and P. E. Hart, Pattern Classification and Scene Analysis, John Wiley and Sons, New York, 1973.

5. E. M. Kennaugh and R. L. Cosgriff, "The Use of Impulse Response in Electromagnetic Scattering Problems," in IRE Nat. Conv. Rec., Part 1, 1958.

6. E. M. Kennaugh and D. L. Moffatt, "Transient and Impulse Response Approximations," Proc. IEEE, Vol. 52, pp. 893-901, August 1965.

7. C. L. Bennett, "A Technique for Computing the Approximate Electromagnetic Impulse Response of Conducting Bodies," Ph.D. Dissertation, Purdue Univ., School of Engineering, Layafette, Indiana, June 1968.

33

8.   Ross, Bates, Susman, Hanley, Smith, and Robbins, "Transient Behavior of Radiating Elements," (AD 812 886).

9.   J. D. Young, "Radar Imaging From Ramp Response Signatures, IEEE Trans. AP-24, No. 3, May 1976, pp. 276-282.

10. K. A. Shubert, J. D. Young, and D. L. Moffatt, "Synthetic Radar Imagery," IEEE Trans. AP-25, No. 4, July 1977, pp. 477-483.

11. L. C. Chan, "Subsurface Electromagnetic Target Characterization and Identification," Report 784722-3, June 1979, The Ohio State University ElectroScience Laboratory, Department of Electrical Engineering; prepared under Contract DAAK70-77-C-0114 for Department of the Army, Ft. Belvoir, Virginia.

12. L. J. White and A. A. Ksienski, "Aircraft Identification Using a Bilinear Surface Representation of Radar Data," Pattern Recognition, Vol. 6, 1974, pp. 35-45.
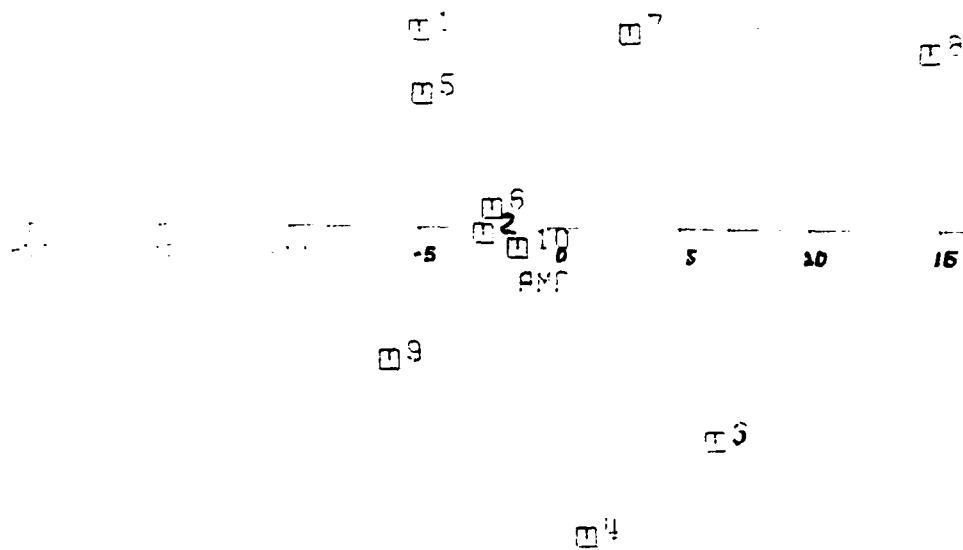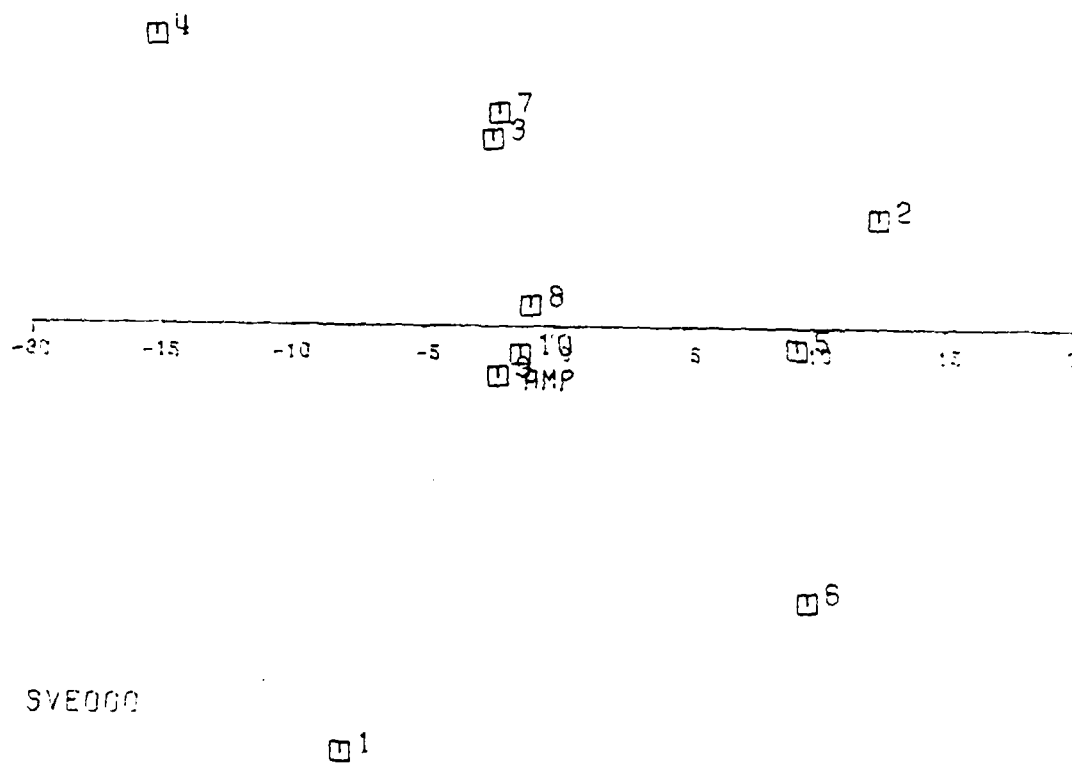
APPENDIX A

The raw data used in the target identification studies presented
in this report is given here. The raw data was in the form of amplitude
and phase measurements of the signal backscattered from a scale model
ship. The ship models used were the Sverdlov and the Missouri (1:700
scale). The amplitude (measured in cm) is given as the square root
of the radar cross section. The phase is given as degrees absolute
with a phase reference determined by a reference sphere. The reference
point for the phase data is a point at the center of the hull of the
ship at the waterline. The Harrington phase reference convention
(increasing distance along the ray path implys decreasing phase values)
is used here.

The values of amplitude and phase are presented as polar plots
so that comparisons between data from various ships or various aspect
angles may be made. The zero phase direction is along the x-axis (to
the right).

The data are given in three groups; bow data, stern data, and
broadside data. The polar plots are identified by a code of the form
MISxxx or SVExxx. The MIS and the SVE part of the identification stand
for Missouri and Sverdlov respectively. The xxx gives the aspect angle
measured in degrees from bow on.

BOW DATA
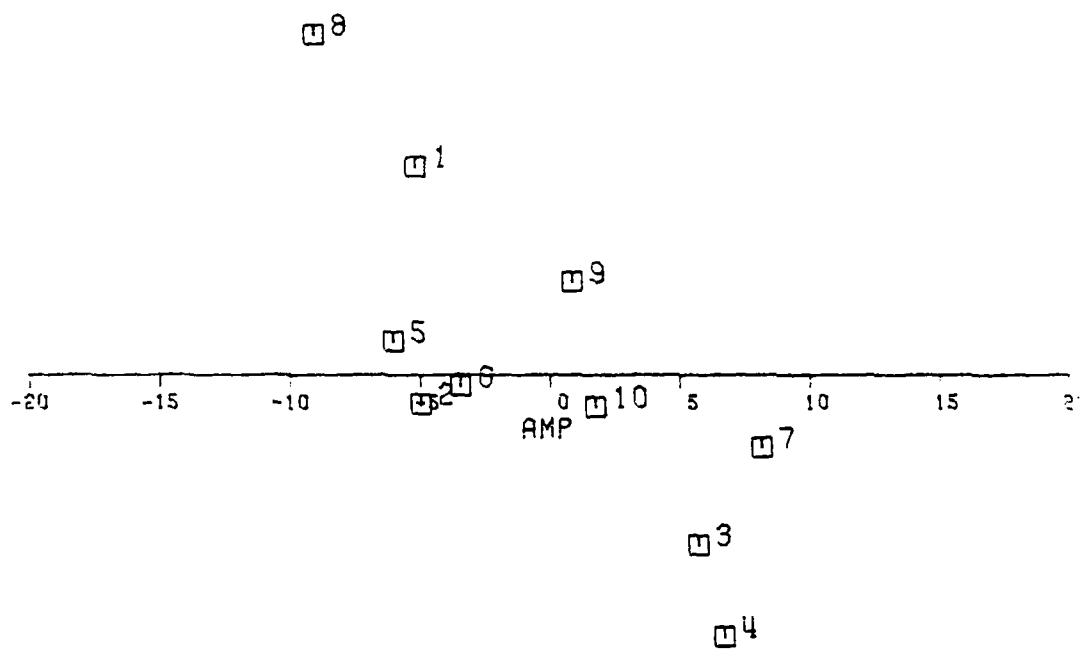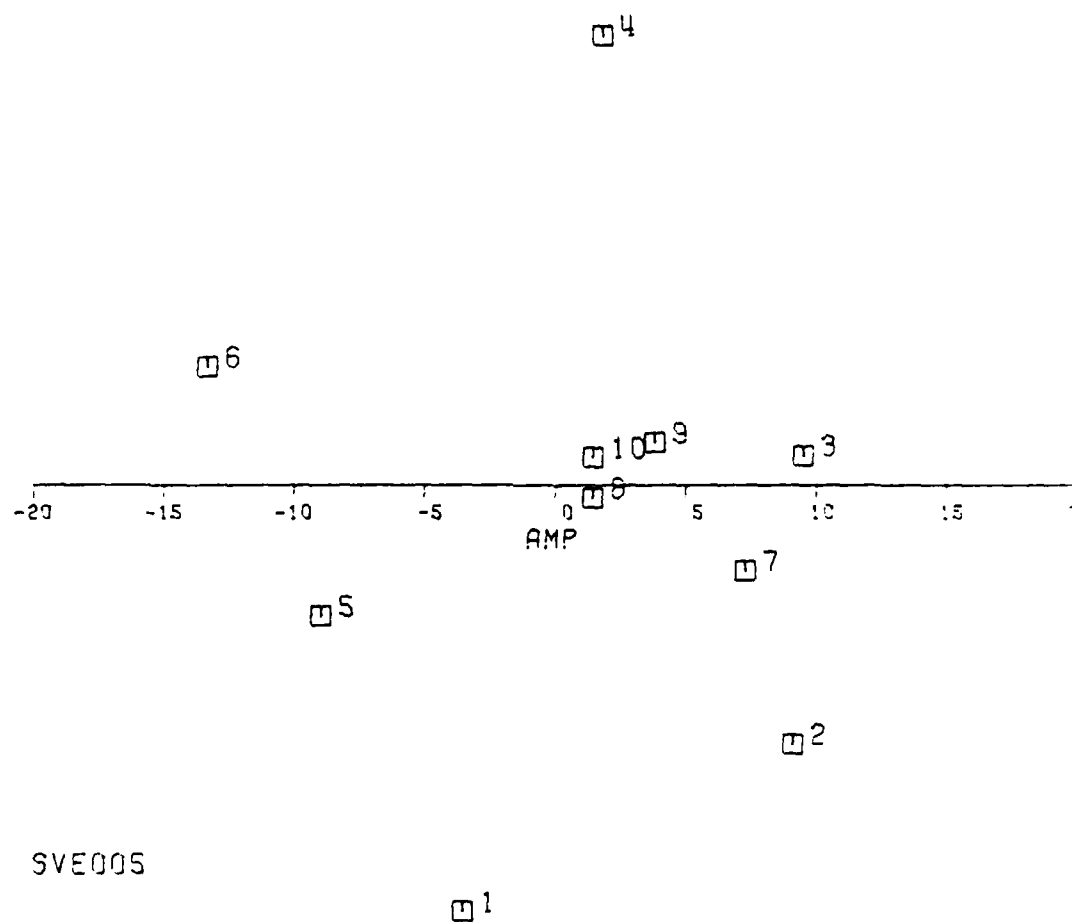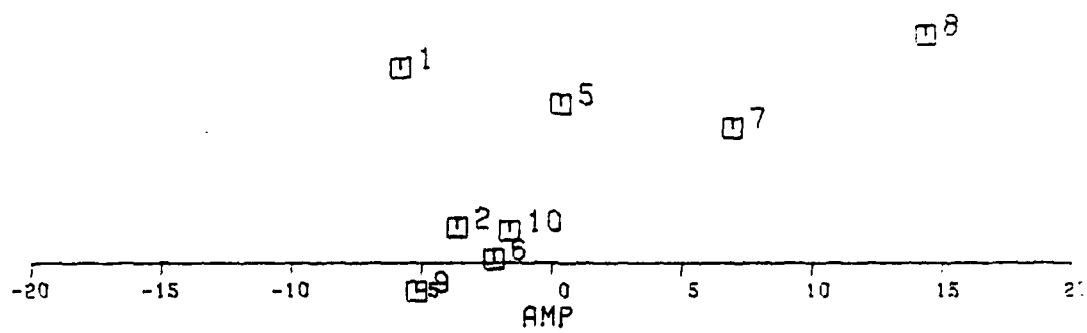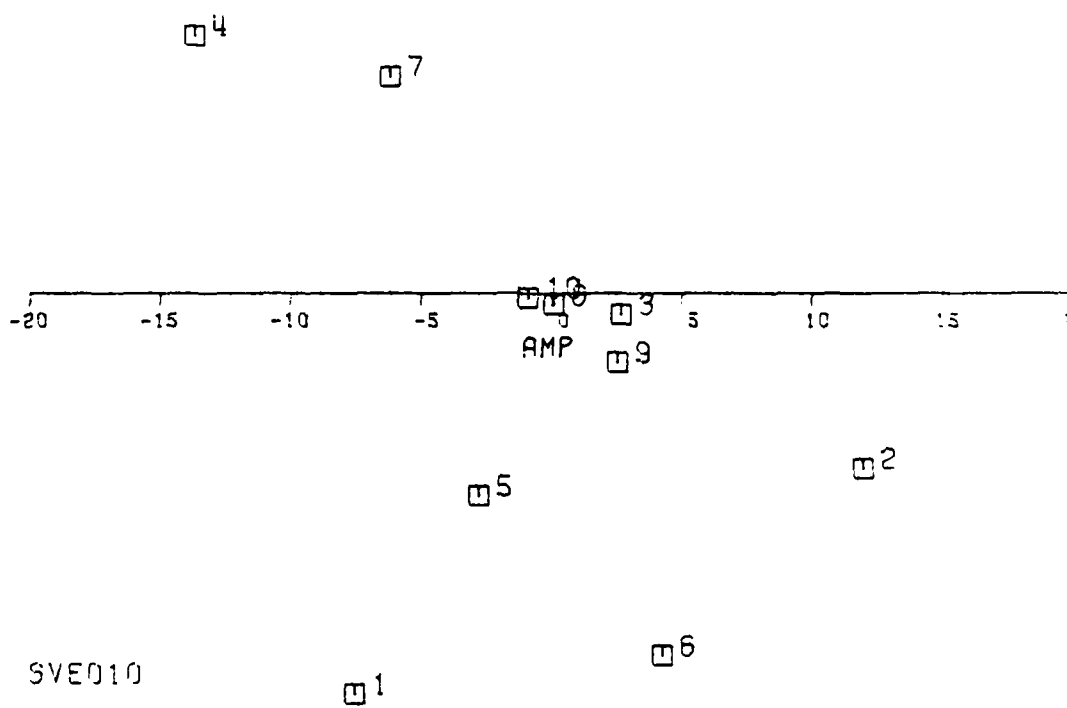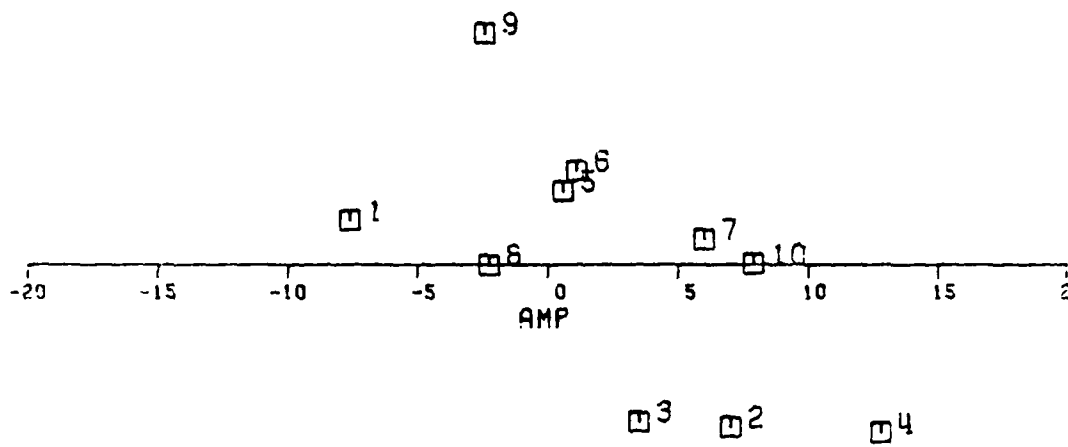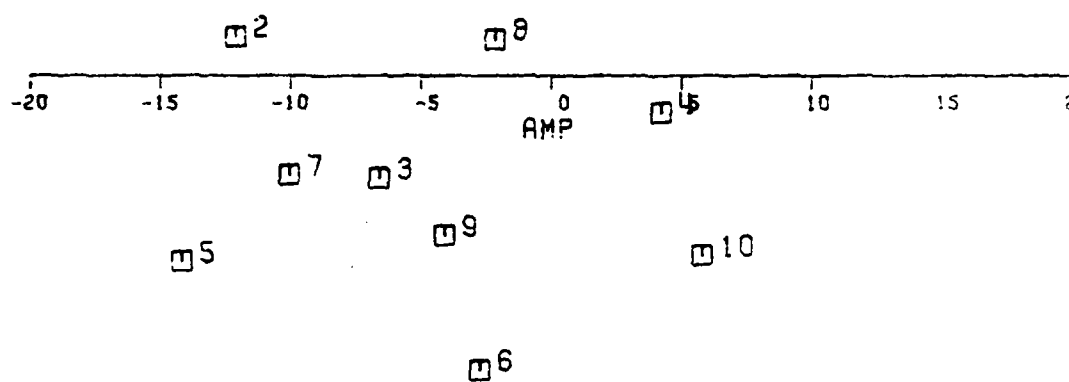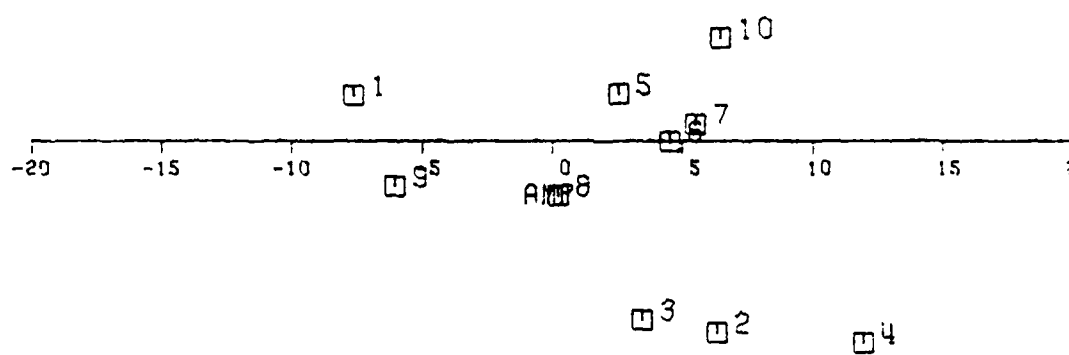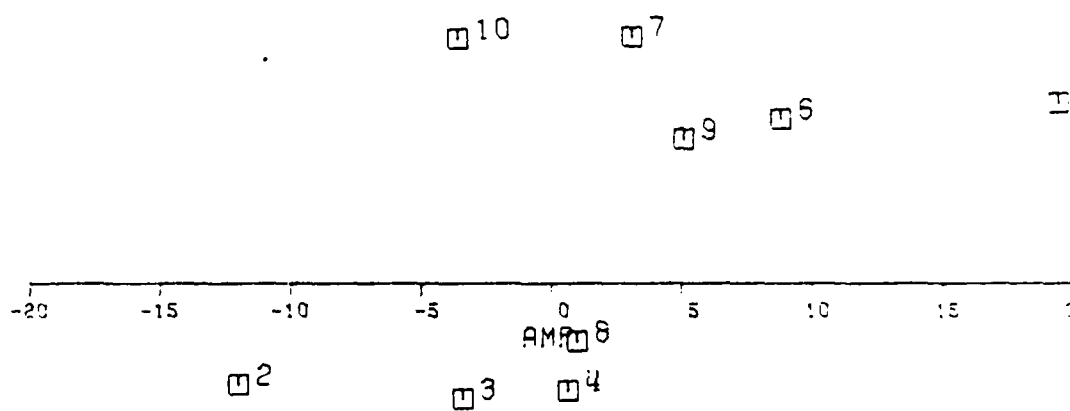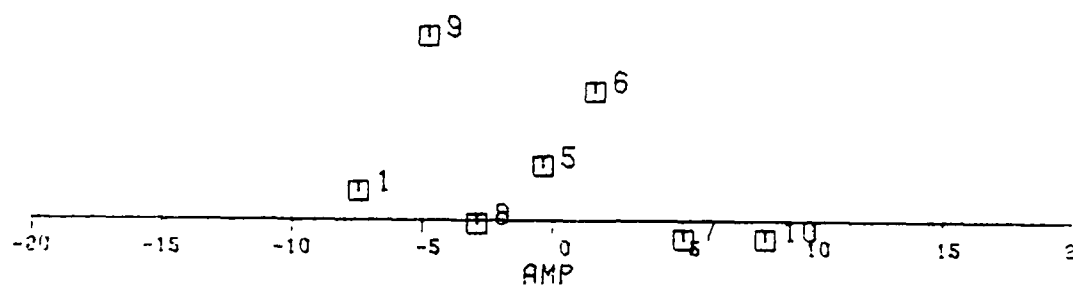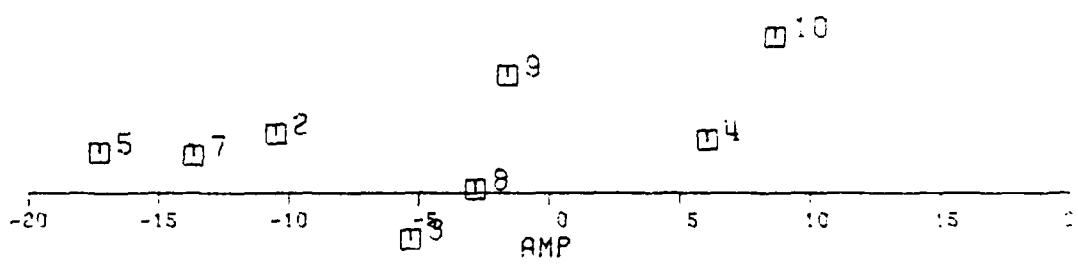
SVE000

MIS005

SVE005

39

MISO10

40

SVE010

AMP

STERN DATA

42

2 8

-20   -15   -10   -5   0   5   10   15   2

AMP

7 3

9

5

10

6

SVE170

1

MI9175

44

□10   □7

□9   □6   H

-20   -15   -10   -5   0   5   10   15

AMP□8

□2

□3   □4

SVE175   □5

45

MI9180

46

SVE180

47

BROADSIDE DATA

MISO30

48

SVF030

49

50

AMP

52

SYE090

53

MIS095

54

AMP

-90   -60   -40   -20   0   20   40   80   9

SVE795

55

2 7

1
3

-80   -60   -40   -20   0   20   40   60   80

AMP

4   5

8   10

8

1

5

9

2

-80   -60   -40   -20   0   20   40   60

AMP

4

3

10

SVF100

6

57
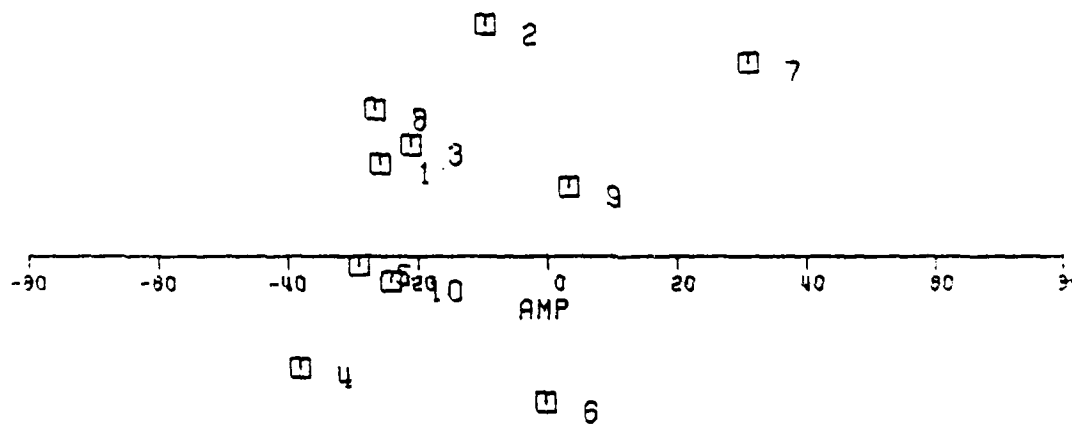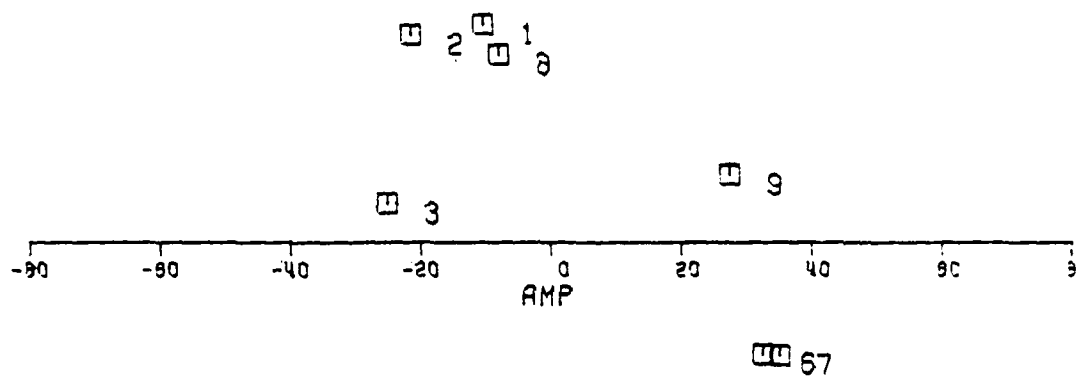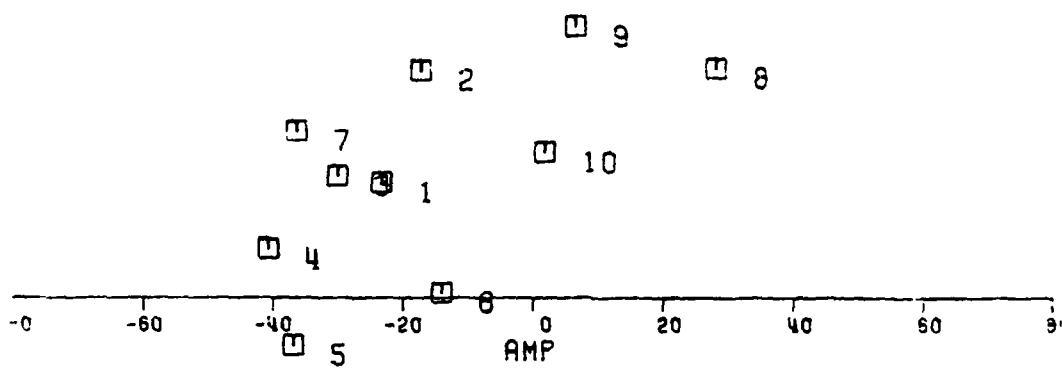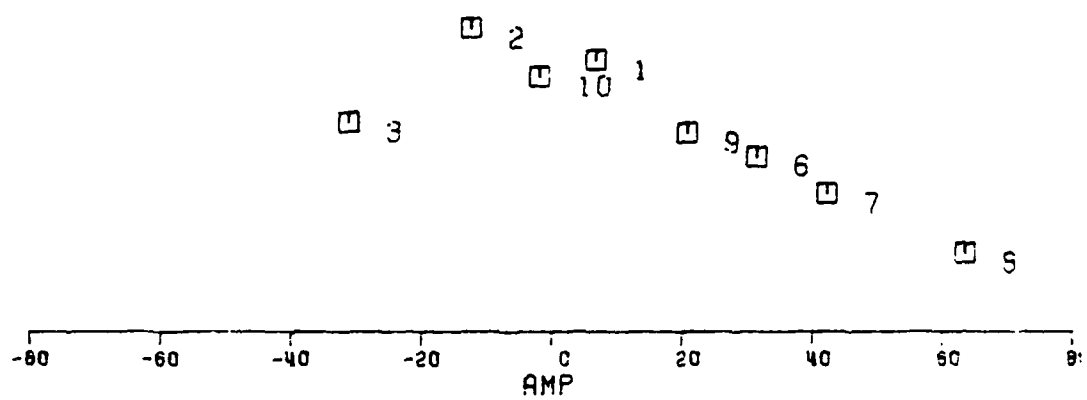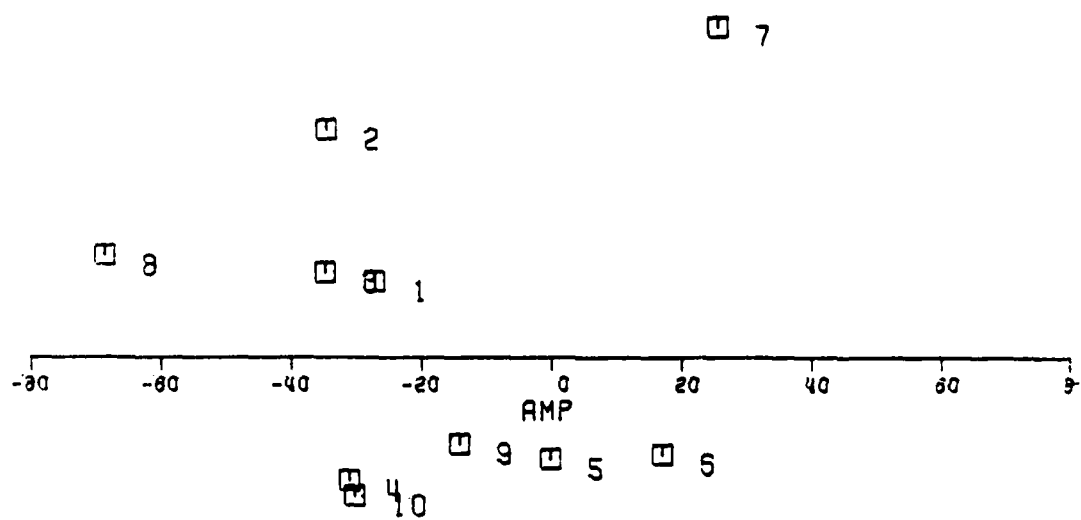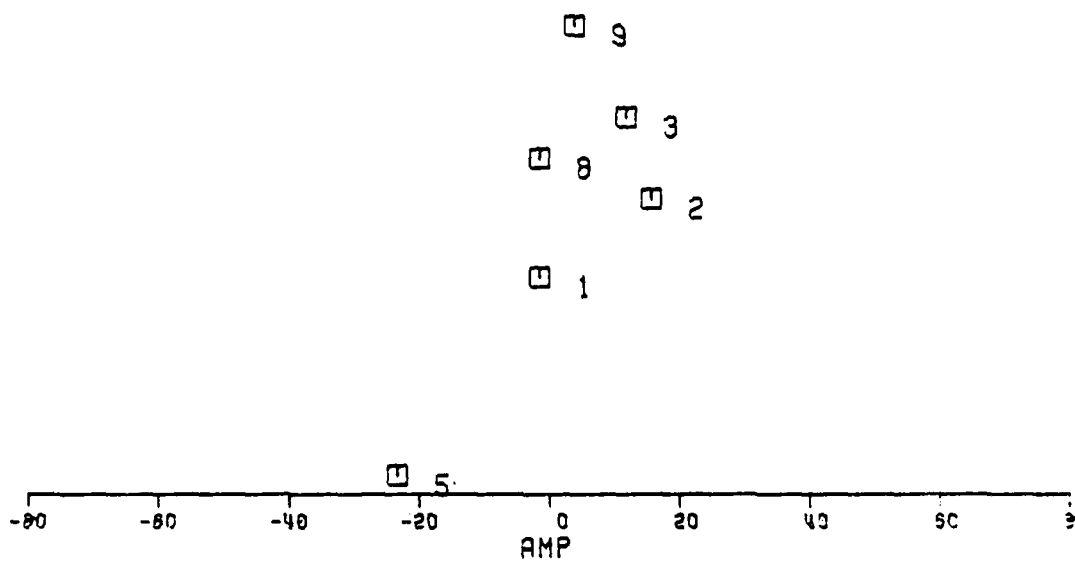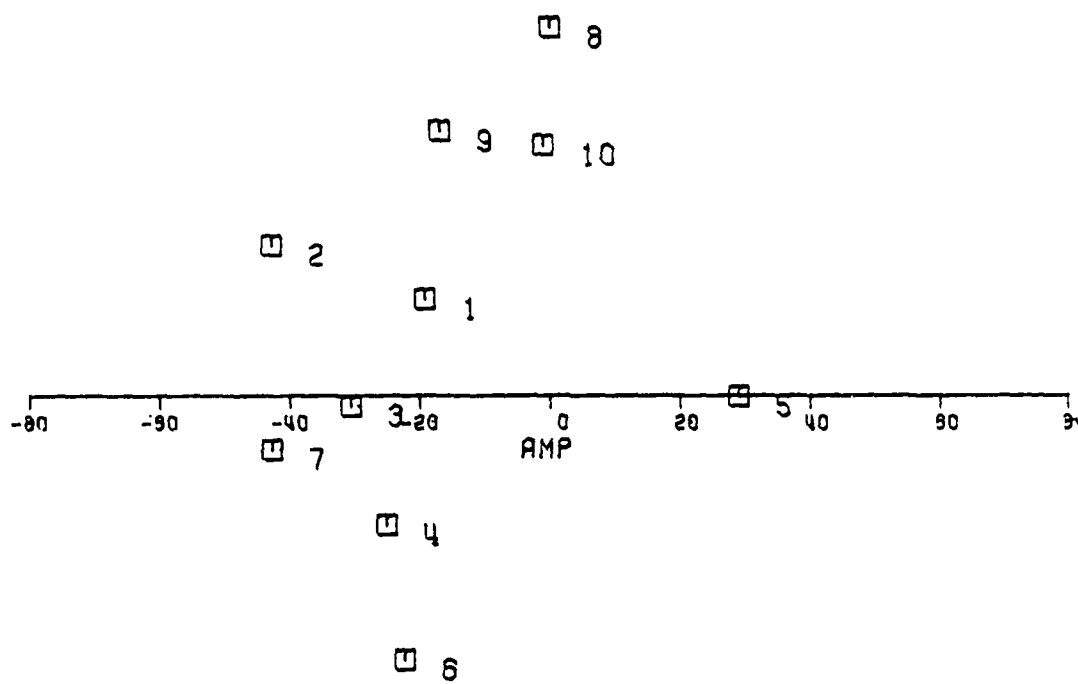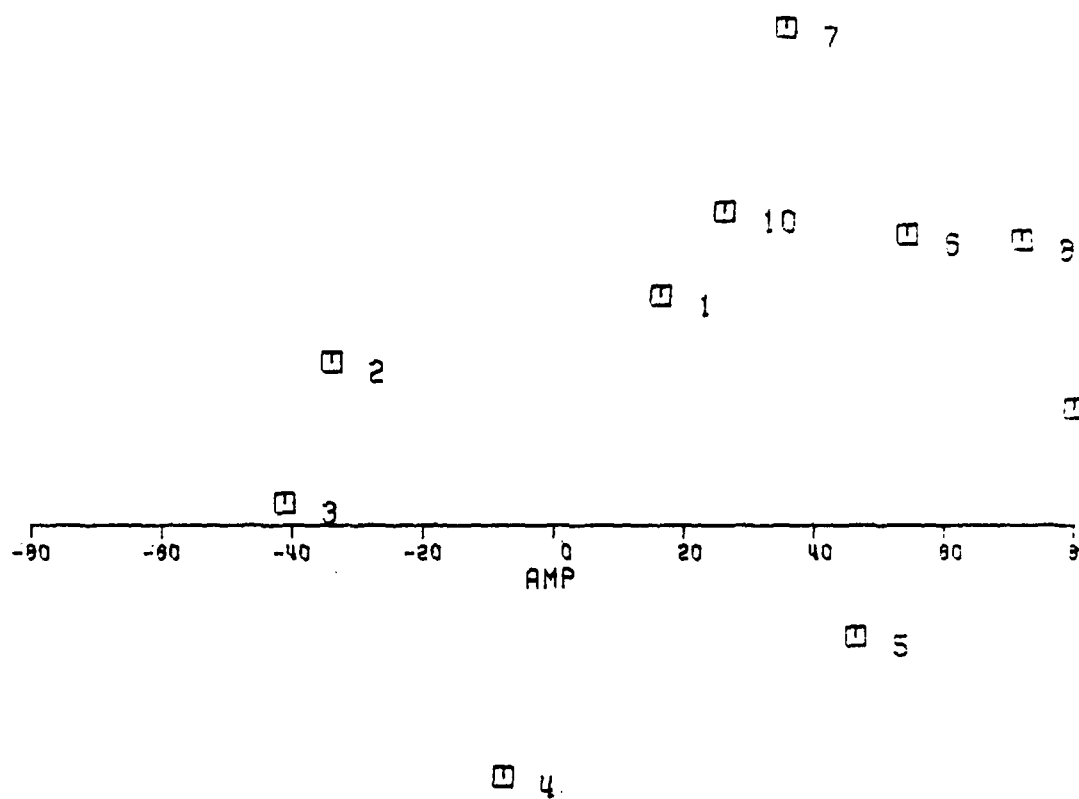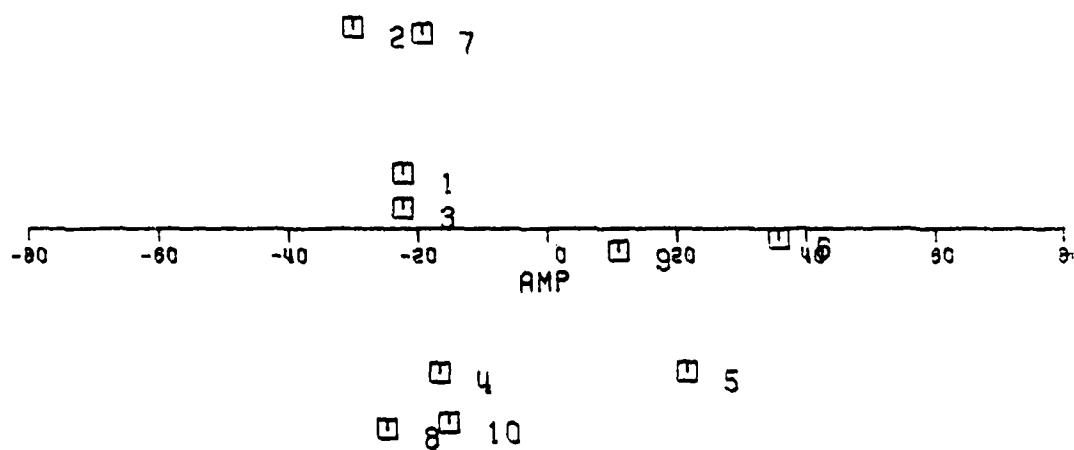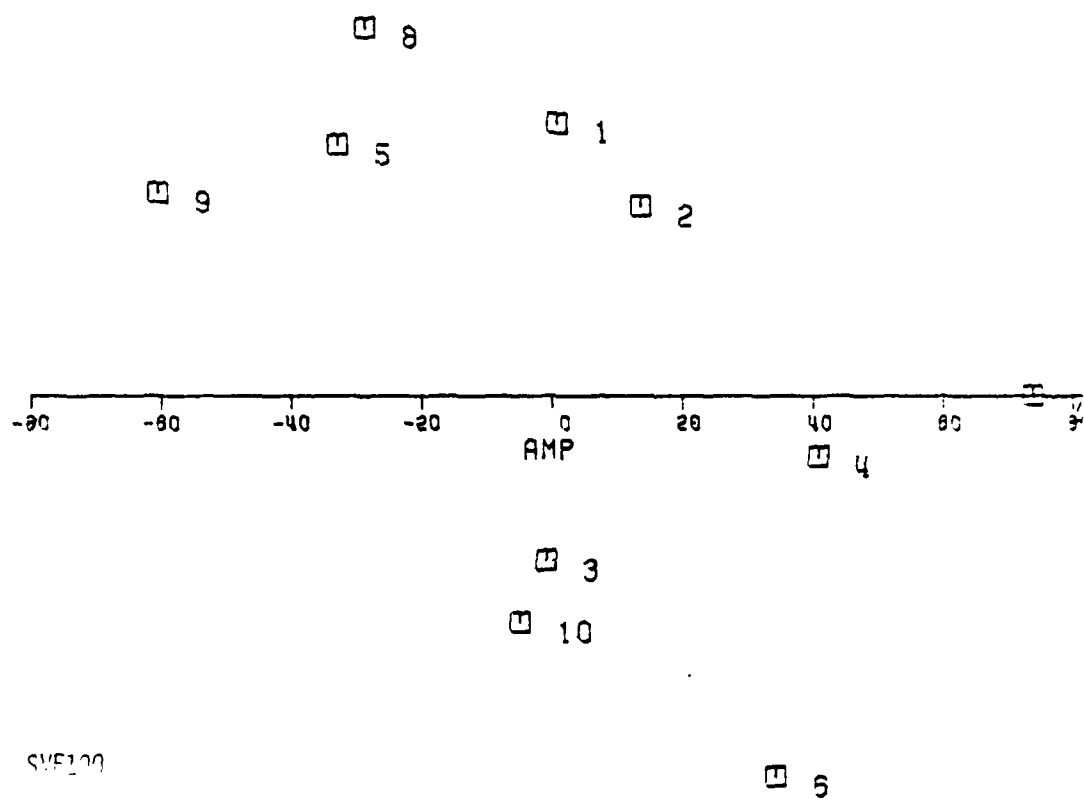
The following tabulations are the nearest neighbor computation
results from this report. They were summarized earlier in this report.
The columns are headed with the code MISxxx or SVExxx. This represents
either the Missouri or the Sverdlov at aspect angle xxx (given in degrees).
The distance (nearest neighbor) from the data for the ship given in
the first column to the data for the ship given at the top of the fol-
lowing columns is printed at the points of intersection. As can be
seen, the distance for identical ship data values is always zero.
The remaining numbers are the result of the nearest neighbor distance
computation. No normalization has been done. The minimum value in
the horizontal row is underlined. It is underlined once if the minimum
is for the same ship and twice if the minimim is for the other ship.
In the upper left are two numbers. The first number is the number
of the first harmonic used in the analysis, and the second number is
the number of the last harmonic used. The numbers are followed by
either a T or an F. The T indicates that phase data has been included
in the computations, and the F indicates that it has not.

The algorithms used for these tabulations is given below.
For amplitude data only:

$$D^2 = \sum_{j=p} (x_j - y_j)^2$$

where:

x_j and y_j are amplitudes of the jth harmonic of two
data sets (x and y)

p is the starting harmonic number

q is the final harmonic number

D^2 is tabulated since a minimum of D^2 implys a minimum
of D.

58

For amplitude and phase data:

$$D^2 = \sum_{j=p}^{q} \left(x_j \sin\theta_{x_j} - y_j \sin\theta_{y_j}\right)^2 + \sum_{j=p}^{q} \left(x_j \cos\theta_{x_j} - y_j \cos\theta_{y_j}\right)^2$$

where:

θ_{x_j} and θ_{y_j} are the phase angles of the jth harmonic of two data sets (x and y).

Top table (T):

	T MIS000	MIS005	MIS010	MIS100	MIS175	MIS170	SVE000	SVE005	SVE010	SVE100	SVE175	SVE170
MIS000	0.00E+00	0.92E+03	0.12E+03	0.89E+03	0.85E+03	0.11E+04	0.28E+04	0.25E+04	0.24E+04	0.37E+04	0.21E+04	0.25E+04
MIS005	0.92E+03	0.00E+00	0.87E+03	0.65E+03	0.85E+03	0.67E+03	0.31E+04	0.22E+04	0.27E+04	0.34E+04	0.20E+04	0.23E+04
MIS010	0.12E+03	0.87E+03	0.00E+00	0.88E+03	0.85E+03	0.10E+04	0.27E+04	0.26E+04	0.25E+04	0.38E+04	0.21E+04	0.27E+04
MIS100	0.89E+03	0.65E+03	0.88E+03	0.00E+00	0.31E+03	0.20E+03	0.24E+04	0.19E+04	0.21E+04	0.34E+04	0.21E+04	0.26E+04
MIS180	0.85E+03	0.85E+03	0.85E+03	0.31E+03	0.00E+00	0.19E+03	0.23E+04	0.19E+04	0.20E+04	0.34E+04	0.22E+04	0.25E+04
MIS175	0.11E+04	0.67E+03	0.10E+04	0.20E+03	0.19E+03	0.00E+00	0.25E+04	0.17E+04	0.22E+04	0.33E+04	0.22E+04	0.26E+04
MIS170	0.28E+04	0.31E+04	0.27E+04	0.24E+04	0.23E+04	0.25E+04	0.00E+00	0.72E+03	0.58E+03	0.35E+04	0.37E+04	0.29E+04
SVE000	0.25E+04	0.22E+04	0.26E+04	0.19E+04	0.19E+04	0.17E+04	0.72E+03	0.00E+00	0.14E+04	0.26E+04	0.31E+04	0.25E+04
SVE005	0.24E+04	0.27E+04	0.25E+04	0.21E+04	0.20E+04	0.22E+04	0.58E+03	0.14E+04	0.00E+00	0.28E+04	0.30E+04	0.22E+04
SVE010	0.37E+04	0.34E+04	0.38E+04	0.34E+04	0.34E+04	0.34E+04	0.35E+04	0.26E+04	0.28E+04	0.00E+00	0.29E+04	0.67E+03
SVE180	0.21E+04	0.21E+04	0.21E+04	0.21E+04	0.22E+04	0.22E+04	0.37E+04	0.31E+04	0.30E+04	0.29E+04	0.22E+04	0.22E+04
SVE175	0.25E+04	0.20E+04	0.27E+04	0.22E+04	0.25E+04	0.26E+04	0.22E+04	0.25E+04	0.22E+04	0.67E+03	0.00E+00	0.22E+04
SVE170	—	—	—	—	—	—	—	—	—	—	—	0.00E+00

Bottom table (F):

	F MIS000	MIS005	MIS010	MIS100	MIS175	MIS170	SVE000	SVE005	SVE010	SVE100	SVE175	SVE170
MIS000	0.00E+00	0.31E+02	0.13E+02	0.31E+02	0.33E+03	0.32E+03	0.65E+03	0.58E+03	0.69E+03	0.13E+04	0.75E+03	0.76E+03
MIS005	0.31E+02	0.00E+00	0.12E+02	0.29E+03	0.28E+03	0.30E+03	0.54E+03	0.49E+03	0.56E+03	0.12E+04	0.69E+03	0.70E+03
MIS010	0.13E+02	0.12E+02	0.00E+00	0.32E+03	0.33E+03	0.34E+03	0.65E+03	0.58E+03	0.69E+03	0.13E+04	0.74E+03	0.74E+03
MIS100	0.31E+03	0.29E+03	0.32E+03	0.00E+00	0.10E+02	0.89E+01	0.39E+03	0.34E+03	0.40E+03	0.12E+04	0.57E+03	0.61E+03
MIS180	0.33E+03	0.28E+03	0.33E+03	0.10E+02	0.00E+00	0.10E+02	0.34E+03	0.29E+03	0.34E+03	0.12E+04	0.54E+03	0.58E+03
MIS175	0.32E+03	0.30E+03	0.34E+03	0.89E+01	0.10E+02	0.00E+00	0.39E+03	0.34E+03	0.40E+03	0.12E+04	0.55E+03	0.58E+03
MIS170	0.65E+03	0.54E+03	0.65E+03	0.39E+03	0.34E+03	0.39E+03	0.00E+00	0.11E+02	0.69E+02	0.71E+03	0.40E+03	0.37E+03
SVE000	0.58E+03	0.49E+03	0.58E+03	0.34E+03	0.29E+03	0.34E+03	0.11E+02	0.00E+00	0.58E+02	0.70E+03	0.35E+03	0.32E+03
SVE005	0.69E+03	0.56E+03	0.69E+03	0.40E+03	0.34E+03	0.40E+03	0.69E+02	0.58E+02	0.00E+00	0.71E+03	0.38E+03	0.37E+03
SVE010	0.13E+04	0.12E+04	0.13E+04	0.12E+04	0.12E+04	0.12E+04	0.71E+03	0.70E+03	0.71E+03	0.00E+00	0.27E+03	0.21E+03
SVE180	0.75E+03	0.69E+03	0.74E+03	0.57E+03	0.54E+03	0.55E+03	0.40E+03	0.35E+03	0.38E+03	0.27E+03	0.00E+00	0.15E+02
SVE175	0.76E+03	0.70E+03	0.74E+03	0.61E+03	0.58E+03	0.58E+03	0.37E+03	0.32E+03	0.37E+03	0.21E+03	0.15E+02	0.00E+00

60

1 5 T

	MIS000	MIS005	MIS010	MIS180	MIS175	MIS170	SVE000	SVE005	SVE010	SVE180	SVE175	SVE170
MIS000	0.00E+00	0.56E+02	0.74E+02	0.20E+03	0.37E+03	0.37E+03	0.22E+04	0.19E+04	0.17E+04	0.27E+04	0.13E+04	0.17E+04
MIS005	0.56E+02	0.00E+00	0.15E+03	0.28E+03	0.32E+03	0.32E+03	0.24E+04	0.18E+04	0.18E+04	0.26E+04	0.11E+04	0.15E+04
MIS010	0.74E+02	0.15E+03	0.00E+00	0.25E+03	0.39E+03	0.41E+03	0.20E+04	0.21E+04	0.18E+04	0.28E+04	0.13E+04	0.17E+04
MIS180	0.20E+03	0.28E+03	0.25E+03	0.00E+00	0.15E+03	0.18E+03	0.17E+04	0.15E+04	0.13E+04	0.28E+04	0.16E+04	0.18E+04
MIS175	0.37E+03	0.32E+03	0.39E+03	0.15E+03	0.00E+00	0.97E+01	0.19E+04	0.14E+04	0.15E+04	0.28E+04	0.17E+04	0.19E+04
MIS170	0.37E+03	0.32E+03	0.41E+03	0.18E+03	0.97E+01	0.00E+00	0.19E+04	0.13E+04	0.14E+04	0.27E+04	0.17E+04	0.18E+04
SVE000	0.22E+04	0.24E+04	0.20E+04	0.17E+04	0.19E+04	0.19E+04	0.00E+00	0.11E+04	0.41E+03	0.28E+04	0.31E+04	0.24E+04
SVE005	0.19E+04	0.18E+04	0.21E+04	0.15E+04	0.14E+04	0.13E+04	0.11E+04	0.00E+00	0.43E+03	0.18E+04	0.23E+04	0.16E+04
SVE010	0.17E+04	0.18E+04	0.18E+04	0.13E+04	0.15E+04	0.14E+04	0.41E+03	0.43E+03	0.00E+00	0.23E+04	0.24E+04	0.19E+04
SVE180	0.27E+04	0.26E+04	0.28E+04	0.28E+04	0.28E+04	0.27E+04	0.28E+04	0.18E+04	0.23E+04	0.00E+00	0.19E+04	0.30E+03
SVE175	0.13E+04	0.11E+04	0.13E+04	0.16E+04	0.17E+04	0.17E+04	0.31E+04	0.23E+04	0.24E+04	0.19E+04	0.00E+00	0.76E+03
SVE170	0.17E+04	0.15E+04	0.17E+04	0.18E+04	0.19E+04	0.18E+04	0.24E+04	0.16E+04	0.19E+04	0.30E+03	0.76E+03	0.00E+00

1 5 F

	MIS000	MIS005	MIS010	MIS180	MIS175	MIS170	SVE000	SVE005	SVE010	SVE180	SVE175	SVE170
MIS000	0.00E+00	0.11E+02	0.45E+01	0.73E+02	0.82E+02	0.83E+02	0.26E+03	0.22E+03	0.27E+03	0.96E+03	0.42E+03	0.43E+03
MIS005	0.11E+02	0.00E+00	0.69E+01	0.38E+02	0.40E+02	0.40E+02	0.28E+03	0.17E+03	0.19E+03	0.90E+03	0.37E+03	0.39E+03
MIS010	0.45E+01	0.69E+01	0.00E+00	0.57E+02	0.66E+02	0.69E+02	0.25E+03	0.21E+03	0.26E+03	0.93E+03	0.39E+03	0.40E+03
MIS180	0.73E+02	0.38E+02	0.57E+02	0.00E+00	0.34E+01	0.49E+01	0.21E+03	0.19E+03	0.20E+03	0.11E+04	0.51E+03	0.53E+03
MIS175	0.82E+02	0.40E+02	0.66E+02	0.34E+01	0.00E+00	0.73E+00	0.18E+03	0.16E+03	0.16E+03	0.11E+04	0.47E+03	0.50E+03
MIS170	0.83E+02	0.40E+02	0.69E+02	0.49E+01	0.73E+00	0.00E+00	0.19E+03	0.16E+03	0.17E+03	0.11E+04	0.48E+03	0.51E+03
SVE000	0.26E+03	0.28E+03	0.25E+03	0.21E+03	0.18E+03	0.19E+03	0.00E+00	0.93E+01	0.30E+02	0.30E+02	0.29E+03	0.28E+03
SVE005	0.22E+03	0.17E+03	0.21E+03	0.19E+03	0.16E+03	0.16E+03	0.93E+01	0.00E+00	0.57E+02	0.50E+02	0.25E+03	0.24E+03
SVE010	0.27E+03	0.19E+03	0.26E+03	0.20E+03	0.16E+03	0.17E+03	0.30E+02	0.57E+02	0.00E+00	0.57E+02	0.26E+03	0.27E+03
SVE180	0.96E+03	0.90E+03	0.93E+03	0.11E+04	0.11E+04	0.11E+04	0.30E+02	0.50E+02	0.57E+02	0.00E+00	0.25E+03	0.18E+03
SVE175	0.42E+03	0.37E+03	0.39E+03	0.51E+03	0.47E+03	0.48E+03	0.29E+03	0.25E+03	0.26E+03	0.25E+03	0.00E+00	0.12E+02
SVE170	0.43E+03	0.39E+03	0.40E+03	0.53E+03	0.50E+03	0.51E+03	0.28E+03	0.24E+03	0.27E+03	0.18E+03	0.12E+02	0.00E+00

3 7 T

	MIS000	MIS005	MIS010	MIS180	MIS175	MIS170	SVE000	SVE005	SVE010	SVE180	SVE175	SVE170
MIS000	0.00E+00	0.18E+03	0.91E+02	0.14E+03	0.30E+03	0.27E+03	0.17E+04	0.13E+04	0.13E+04	0.95E+03	0.74E+03	0.99E+03
MIS005	0.18E+03	0.00E+00	0.21E+03	0.14E+03	0.19E+03	0.16E+03	0.19E+04	0.10E+04	0.10E+04	0.96E+03	0.80E+03	0.82E+03
MIS010	0.91E+02	0.21E+03	0.00E+00	0.13E+03	0.25E+03	0.25E+03	0.15E+04	0.14E+04	0.14E+04	0.11E+04	0.81E+03	0.11E+04
MIS180	0.14E+03	0.14E+03	0.13E+03	0.00E+00	0.19E+03	0.19E+03	0.17E+04	0.14E+04	0.15E+04	0.13E+04	0.69E+03	0.11E+04
MIS175	0.30E+03	0.19E+03	0.25E+03	0.19E+03	0.00E+00	0.33E+02	0.16E+04	0.14E+04	0.15E+04	0.12E+04	0.73E+03	0.10E+04
MIS170	0.27E+03	0.16E+03	0.25E+03	0.19E+03	0.33E+02	0.00E+00	0.18E+04	0.12E+04	0.16E+04	0.11E+04	0.74E+03	0.10E+04
SVE000	0.17E+04	0.19E+04	0.15E+04	0.17E+04	0.16E+04	0.18E+04	0.00E+00	0.19E+04	0.35E+03	0.18E+04	0.15E+04	0.16E+04
SVE005	0.13E+04	0.10E+04	0.14E+04	0.14E+04	0.14E+04	0.12E+04	0.19E+04	0.00E+00	0.14E+04	0.13E+04	0.14E+04	0.13E+04
SVE010	0.13E+04	0.10E+04	0.11E+04	0.15E+04	0.15E+04	0.16E+04	0.35E+03	0.14E+04	0.00E+00	0.11E+04	0.11E+04	0.89E+03
SVE180	0.95E+03	0.96E+03	0.11E+04	0.13E+04	0.12E+04	0.11E+04	0.18E+04	0.13E+04	0.11E+04	0.00E+00	0.12E+04	0.17E+03
SVE175	0.74E+03	0.80E+03	0.81E+03	0.69E+03	0.73E+03	0.74E+03	0.15E+04	0.14E+04	0.11E+04	0.12E+04	0.00E+00	0.92E+03
SVE170	0.99E+03	0.82E+03	0.11E+04	0.11E+04	0.10E+04	0.10E+04	0.16E+04	0.13E+04	0.89E+03	0.17E+03	0.92E+03	0.00E+00

3 7 F

	MIS000	MIS005	MIS010	MIS180	MIS175	MIS170	SVE000	SVE005	SVE010	SVE180	SVE175	SVE170
MIS000	0.00E+00	0.56E+01	0.30E+01	0.48E+02	0.40E+02	0.41E+02	0.21E+03	0.18E+03	0.24E+03	0.24E+03	0.26E+03	0.24E+03
MIS005	0.56E+01	0.00E+00	0.69E+01	0.35E+02	0.26E+02	0.25E+02	0.18E+03	0.16E+03	0.19E+03	0.23E+03	0.24E+03	0.22E+03
MIS010	0.30E+01	0.69E+01	0.00E+00	0.50E+02	0.45E+02	0.45E+02	0.23E+03	0.20E+03	0.26E+03	0.25E+03	0.26E+03	0.23E+03
MIS180	0.48E+02	0.35E+02	0.50E+02	0.00E+00	0.33E+01	0.78E+01	0.18E+03	0.17E+03	0.20E+03	0.39E+03	0.38E+03	0.35E+03
MIS175	0.40E+02	0.26E+02	0.45E+02	0.33E+01	0.00E+00	0.14E+01	0.17E+03	0.16E+03	0.18E+03	0.36E+03	0.36E+03	0.34E+03
MIS170	0.41E+02	0.25E+02	0.45E+02	0.78E+01	0.14E+01	0.00E+00	0.18E+03	0.18E+03	0.19E+03	0.37E+03	0.37E+03	0.35E+03
SVE000	0.21E+03	0.18E+03	0.23E+03	0.18E+03	0.17E+03	0.18E+03	0.00E+00	0.73E+01	0.32E+01	0.28E+03	0.30E+03	0.27E+03
SVE005	0.18E+03	0.16E+03	0.20E+03	0.17E+03	0.16E+03	0.18E+03	0.73E+01	0.00E+00	0.56E+02	0.24E+03	0.25E+03	0.22E+03
SVE010	0.24E+03	0.19E+03	0.26E+03	0.20E+03	0.18E+03	0.19E+03	0.32E+01	0.56E+02	0.00E+00	0.24E+03	0.26E+03	0.25E+03
SVE180	0.24E+03	0.23E+03	0.25E+03	0.39E+03	0.36E+03	0.37E+03	0.28E+03	0.24E+03	0.24E+03	0.00E+00	0.21E+02	0.24E+02
SVE175	0.26E+03	0.24E+03	0.26E+03	0.38E+03	0.36E+03	0.37E+03	0.30E+03	0.25E+03	0.26E+03	0.21E+02	0.00E+00	0.72E+01
SVE170	0.24E+03	0.22E+03	0.23E+03	0.35E+03	0.34E+03	0.35E+03	0.27E+03	0.22E+03	0.25E+03	0.24E+02	0.72E+01	0.00E+00

6 10 T

	MIS000	MIS005	MIS010	MIS180	MIS175	MIS170	SVE000	SVE005	SVE010	SVE180	SVE175	SVE170
MIS000	0.00E+00	0.87E+03	0.46E+02	0.70E+03	0.48E+03	0.69E+03	0.60E+03	0.65E+03	0.68E+··	0.10E+04	0.77E+03	0.84E+03
MIS005	0.87E+20	0.00E+00	0.72E+03	0.37E+03	0.53E+03	0.35E+03	0.77E+03	0.44E+03	0.89E+03	0.86E+·3	0.88E+03	0.00E+03
MIS010	0.46E+02	0.72E+03	0.00E+00	0.62E+03	0.46E+03	0.60E+03	0.67E+03	0.57E+·3	0.78E+03	0.11E+04	0.72E+03	0.98E+03
MIS180	0.70E+03	0.37E+03	0.62E+03	0.00E+00	0.15E+03	0.16E+02	0.62E+03	0.41E+03	0.81E+03	0.63E+03	0.52E+03	0.74E+03
MIS175	0.48E+03	0.53E+03	0.46E+03	0.15E+03	0.00E+00	0.18E+03	0.37E+03	0.50E+03	0.54E+03	0.62E+03	0.45E+03	0.60E+03
MIS170	0.69E+03	0.35E+03	0.60E+03	0.16E+02	0.18E+03	0.00E+00	0.60E+03	0.38E+03	0.76E+03	0.62E+03	0.45E+03	0.80E+03
SVE000	0.60E+03	0.77E+03	0.67E+03	0.62E+03	0.37E+03	0.60E+03	0.00E+00	0.11E+04	0.85E+02	0.63E+03	0.55E+03	0.47E+03
SVE005	0.65E+03	0.44E+03	0.57E+03	0.41E+03	0.50E+03	0.65E+03	0.11E+04	0.00E+00	0.10E+04	0.79E+03	0.79E+03	0.89E+03
SVE010	0.68E+03	0.89E+03	0.78E+03	0.81E+03	0.54E+03	0.68E+03	0.85E+02	0.10E+04	0.00E+00	0.46E+03	0.70E+03	0.37E+03
SVE180	0.10E+04	0.86E+03	0.11E+04	0.63E+03	0.62E+03	0.10E+04	0.63E+03	0.79E+03	0.46E+03	0.00E+00	0.98E+03	0.36E+03
SVE175	0.77E+03	0.88E+03	0.72E+03	0.52E+03	0.45E+03	0.77E+03	0.55E+03	0.79E+03	0.70E+03	0.98E+03	0.00E+00	0.14E+04
SVE170	0.84E+03	0.00E+03	0.98E+03	0.74E+03	0.60E+03	0.80E+03	0.47E+03	0.89E+03	0.37E+03	0.36E+03	0.14E+04	0.00E+00

6 10 F

	MIS000	MIS005	MIS010	MIS180	MIS175	MIS170	SVE000	SVE005	SVE010	SVE180	SVE175	SVE170
MIS000	0.00E+00	0.21E+02	0.85E+01	0.24E+03	0.25E+03	0.24E+03	0.39E+03	0.36E+03	0.42E+03	0.35E+03	0.34E+03	0.33E+03
MIS005	0.21E+02	0.00E+00	0.50E+01	0.25E+03	0.24E+03	0.26E+03	0.34E+03	0.32E+03	0.37E+03	0.31E+03	0.32E+03	0.31E+03
MIS010	0.85E+01	0.50E+01	0.00E+00	0.26E+03	0.26E+03	0.27E+03	0.40E+03	0.38E+03	0.43E+03	0.35E+03	0.35E+03	0.35E+03
MIS180	0.24E+03	0.25E+03	0.26E+03	0.00E+00	0.69E+01	0.40E+01	0.18E+03	0.15E+03	0.20E+03	0.11E+03	0.61E+02	0.76E+02
MIS175	0.25E+03	0.24E+03	0.26E+03	0.69E+01	0.00E+00	0.94E+01	0.14E+03	0.14E+03	0.18E+03	0.10E+03	0.68E+02	0.82E+02
MIS170	0.24E+03	0.26E+03	0.27E+03	0.40E+01	0.94E+01	0.00E+00	0.16E+03	0.17E+03	0.22E+03	0.12E+03	0.74E+02	0.89E+02
SVE000	0.39E+03	0.34E+03	0.40E+03	0.18E+03	0.16E+03	0.20E+03	0.00E+00	0.22E+01	0.53E+01	0.14E+03	0.11E+03	0.89E+02
SVE005	0.36E+03	0.32E+03	0.38E+03	0.15E+03	0.14E+03	0.17E+03	0.22E+01	0.00E+00	0.82E+01	0.13E+03	0.96E+02	0.76E+02
SVE010	0.42E+03	0.37E+03	0.43E+03	0.20E+03	0.18E+03	0.22E+03	0.53E+01	0.82E+01	0.00E+00	0.14E+03	0.12E+03	0.92E+02
SVE180	0.35E+03	0.31E+03	0.35E+03	0.11E+03	0.10E+03	0.12E+03	0.14E+03	0.13E+03	0.14E+03	0.00E+00	0.24E+02	0.23E+02
SVE175	0.34E+03	0.32E+03	0.35E+03	0.61E+02	0.68E+02	0.74E+02	0.11E+03	0.96E+02	0.12E+03	0.24E+02	0.00E+00	0.26E+00
SVE170	0.33E+03	0.31E+03	0.35E+03	0.76E+02	0.82E+02	0.89E+02	0.89E+02	0.76E+02	0.92E+02	0.23E+02	0.26E+01	0.00E+00

3	7	T	MIS080	MIS085	MIS090	MIS095	MIS100	SVE080	SVE085	SVE090	SVE095	SVE100
		MIS080	0.00E+00	0.61E+04	0.21E+04	0.12E+04	0.80E+04	0.87E+04	0.94E+04	0.13E+05	0.18E+05	0.15E+05
		MIS085	0.61E+04	0.00E+00	0.80E+04	0.88E+04	0.82E+04	0.17E+05	0.17E+05	0.17E+05	0.25E+05	0.31E+05
		MIS090	0.21E+04	0.80E+04	0.00E+00	0.12E+05	0.39E+04	0.73E+04	0.62E+04	0.18E+05	0.89E+04	0.19E+05
		MIS095	0.12E+04	0.88E+04	0.12E+05	0.03E+00	0.76E+04	0.13E+05	0.21E+05	0.15E+05	0.28E+05	0.28E+05
		MIS100	0.80E+04	0.82E+04	0.39E+04	0.76E+04	0.00E+00	0.68E+04	0.72E+04	0.17E+05	0.90E+04	0.24E+05
		SVE080	0.87E+04	0.37E+04	0.73E+04	0.13E+05	0.68E+04	0.00E+00	0.46E+04	0.12E+05	0.16E+05	0.18E+05
		SVE085	0.94E+04	0.17E+05	0.62E+04	0.21E+05	0.72E+04	0.46E+04	0.00E+00	0.20E+05	0.75E+04	0.23E+05
		SVE090	0.13E+05	0.17E+05	0.18E+05	0.15E+05	0.17E+05	0.12E+05	0.20E+05	0.00E+00	0.49E+05	0.22E+05
		SVE095	0.18E+05	0.25E+05	0.89E+04	0.28E+05	0.90E+04	0.16E+05	0.75E+04	0.40E+05	0.00E+00	0.33E+05
		SVE100	0.15E+05	0.31E+05	0.19E+05	0.28E+05	0.24E+05	0.18E+05	0.23E+05	0.22E+05	0.33E+05	0.00E+00

3	7	F	MIS080	MIS085	MIS090	MIS095	MIS100	SVE080	SVE085	SVE090	SVE095	SVE100
		MIS080	0.00E+00	0.21E+03	0.51E+03	0.68E+03	0.45E+03	0.62E+03	0.85E+03	0.23E+04	0.46E+04	0.35E+04
		MIS085	0.21E+03	0.00E+00	0.74E+03	0.12E+04	0.95E+03	0.77E+03	0.86E+03	0.26E+04	0.49E+04	0.40E+04
		MIS090	0.51E+03	0.74E+03	0.00E+00	0.98E+03	0.11E+04	0.18E+04	0.12E+04	0.16E+04	0.42E+04	0.37E+04
		MIS095	0.68E+03	0.12E+04	0.98E+03	0.00E+00	0.26E+03	0.66E+03	0.47E+03	0.11E+04	0.28E+04	0.26E+04
		MIS100	0.45E+03	0.95E+03	0.11E+04	0.26E+03	0.00E+00	0.57E+03	0.92E+03	0.23E+04	0.44E+04	0.31E+04
		SVE080	0.62E+03	0.77E+03	0.18E+04	0.66E+03	0.57E+03	0.00E+00	0.51E+03	0.24E+04	0.34E+04	0.22E+04
		SVE085	0.85E+03	0.86E+03	0.12E+04	0.47E+03	0.92E+03	0.51E+03	0.00E+00	0.81E+03	0.23E+04	0.19E+04
		SVE090	0.23E+04	0.26E+04	0.16E+04	0.11E+04	0.23E+04	0.24E+04	0.81E+03	0.00E+00	0.20E+04	0.23E+04
		SVE095	0.46E+04	0.49E+04	0.42E+04	0.28E+04	0.44E+04	0.34E+04	0.23E+04	0.20E+04	0.00E+00	0.38E+03
		SVE100	0.35E+04	0.40E+04	0.37E+04	0.20E+04	0.31E+04	0.22E+04	0.19E+04	0.23E+04	0.38E+03	0.00E+00

64

6 10 T

	MIS080	MIS085	MIS090	MIS095	MIS100	SVE080	SVE085	SVE090	SVE095	SVE100
MIS080	0.00E+00	0.11E+05	0.38E+04	0.13E+05	0.82E+04	0.61E+04	0.15E+05	0.16E+05	0.31E+05	0.12E+05
MIS085	0.11E+05	0.00E+00	0.22E+05	0.50E+04	0.15E+05	0.16E+05	0.11E+05	0.19E+05	0.24E+05	0.30E+05
MIS090	0.38E+04	0.22E+05	0.00E+00	0.24E+05	0.81E+04	0.12E+05	0.28E+05	0.27E+05	0.44E+05	0.15E+05
MIS095	0.13E+05	0.50E+04	0.24E+05	0.00E+00	0.23E+05	0.19E+05	0.23E+05	0.14E+05	0.43E+05	0.25E+05
MIS100	0.82E+04	0.15E+05	0.81E+04	0.23E+05	0.00E+00	0.10E+05	0.21E+05	0.24E+05	0.36E+05	0.27E+05
SVE080	0.61E+04	0.16E+05	0.12E+05	0.19E+05	0.10E+05	0.00E+00	0.15E+05	0.11E+05	0.31E+05	0.13E+05
SVE085	0.15E+05	0.11E+05	0.28E+05	0.23E+05	0.21E+05	0.15E+05	0.00E+00	0.27E+05	0.96E+04	0.31E+05
SVE090	0.16E+05	0.19E+05	0.27E+05	0.14E+05	0.24E+05	0.11E+05	0.27E+05	0.00E+00	0.53E+05	0.17E+05
SVE095	0.31E+05	0.24E+05	0.44E+05	0.43E+05	0.36E+05	0.31E+05	0.96E+04	0.53E+05	0.00E+00	0.57E+05
SVE100	0.12E+05	0.30E+05	0.15E+05	0.25E+05	0.27E+05	0.13E+05	0.31E+05	0.17E+05	0.57E+05	0.00E+00

6 10 F

	MIS080	MIS085	MIS090	MIS095	MIS100	SVE080	SVE085	SVE090	SVE095	SVE100
MIS080	0.00E+00	0.11E+04	0.17E+04	0.23E+04	0.33E+04	0.78E+03	0.21E+04	0.59E+04	0.12E+05	0.72E+04
MIS085	0.11E+04	0.00E+00	0.16E+04	0.14E+04	0.16E+04	0.12E+04	0.14E+04	0.36E+04	0.90E+04	0.49E+04
MIS090	0.17E+04	0.16E+04	0.00E+00	0.15E+04	0.16E+04	0.22E+04	0.79E+03	0.44E+04	0.76E+04	0.48E+04
MIS095	0.23E+04	0.14E+04	0.15E+04	0.00E+00	0.15E+04	0.10E+04	0.15E+03	0.12E+04	0.48E+04	0.20E+04
MIS100	0.33E+03	0.16E+04	0.16E+04	0.15E+04	0.00E+00	0.45E+04	0.15E+04	0.49E+04	0.11E+05	0.63E+04
SVE080	0.78E+03	0.12E+04	0.22E+04	0.10E+04	0.45E+03	0.00E+00	0.14E+04	0.31E+04	0.92E+04	0.48E+04
SVE085	0.21E+04	0.14E+04	0.79E+03	0.15E+03	0.15E+04	0.14E+04	0.00E+00	0.18E+04	0.49E+04	0.24E+04
SVE090	0.59E+04	0.36E+04	0.44E+04	0.12E+04	0.49E+04	0.31E+04	0.18E+04	0.00E+00	0.22E+04	0.87E+03
SVE095	0.12E+05	0.90E+04	0.76E+04	0.48E+04	0.11E+05	0.92E+04	0.49E+04	0.22E+04	0.00E+00	0.11E+04
SVE100	0.72E+04	0.49E+04	0.48E+04	0.20E+04	0.63E+04	0.48E+04	0.24E+04	0.87E+03	0.11E+04	0.00E+00

	1	5	T MIS080	MIS085	MIS090	MIS095	MIS100	SVE080	SVE085	SVE090	SVE095	SVE100
MIS080			0.00E+00	0.10E+03	0.25E+03	0.00E+00	0.42E+04	0.61E+04	0.47E+04	0.47E+04	0.11E+05	0.12E+05
MIS085			0.10E+03	0.00E+00	0.25E+03	0.16E+04	0.57E+04	0.79E+04	0.93E+04	0.63E+04	0.13E+05	0.14E+05
MIS090			0.32E+04	0.00E+00	0.16E+04	0.00E+00	0.10E+04	0.33E+04	0.57E+04	0.89E+04	0.58E+04	0.16E+05
MIS095			0.53E+04	0.16E+04	0.00E+00	0.09E+05	0.93E+03	0.48E+04	0.79E+04	0.13E+05	0.32E+04	0.16E+05
MIS100			0.42E+04	0.57E+04	0.18E+04	0.98E+03	0.21E+04	0.21E+04	0.56E+04	0.10E+05	0.36E+04	0.15E+05
SVE080			0.61E+04	0.75E+04	0.33E+04	0.21E+04	0.00E+00	0.00E+00	0.18E+04	0.10E+05	0.36E+04	0.16E+05
SVE085			0.77E+04	0.93E+04	0.57E+04	0.79E+04	0.59E+04	0.18E+04	0.00E+00	0.75E+04	0.46E+04	0.15E+05
SVE090			0.47E+04	0.69E+04	0.89E+04	0.13E+05	0.10E+05	0.10E+05	0.76E+04	0.00E+00	0.15E+05	0.14E+05
SVE095			0.11E+05	0.13E+05	0.58E+04	0.36E+04	0.36E+04	0.36E+04	0.46E+04	0.15E+05	0.00E+00	0.18E+05
SVE100			0.12E+05	0.14E+05	0.16E+05	0.16E+05	0.15E+05	0.15E+05	0.15E+05	0.14E+05	0.18E+05	0.00E+00

	1	5	F MIS080	MIS085	MIS090	MIS095	MIS100	SVE080	SVE085	SVE090	SVE095	SVE100
MIS080			0.00E+00	0.14E+03	0.00E+00	0.46E+03	0.27E+03	0.29E+03	0.44E+03	0.76E+03	0.12E+04	0.72E+03	0.64E+03
MIS085			0.14E+03	0.00E+00	0.62E+03	0.31E+03	0.31E+03	0.45E+03	0.26E+03	0.36E+03	0.85E+03	0.27E+03	0.73E+03
MIS090			0.46E+03	0.62E+03	0.00E+00	0.26E+03	0.45E+03	0.59E+03	0.93E+03	0.57E+03	0.13E+04	0.19E+04	0.22E+04
MIS095			0.27E+03	0.31E+03	0.26E+03	0.00E+00	0.59E+03	0.75E+03	0.98E+03	0.84E+03	0.10E+04	0.38E+03
MIS100			0.29E+03	0.26E+03	0.12E+03	0.00E+00	0.00E+00	0.71E+03	0.11E+04	0.12E+03	0.11E+04	0.11E+04	0.10E+04
SVE080			0.44E+03	0.77E+03	0.59E+03	0.12E+03	0.00E+00	0.00E+00	0.57E+03	0.16E+04	0.19E+04	0.27E+04
SVE085			0.76E+03	0.36E+03	0.14E+04	0.77E+03	0.71E+03	0.57E+03	0.00E+00	0.62E+03	0.00E+00	0.12E+04	0.91E+02
SVE090			0.12E+04	0.85E+03	0.57E+03	0.75E+03	0.11E+04	0.00E+00	0.19E+04	0.00E+00	0.10E+04	0.73E+03
SVE095			0.72E+03	0.57E+03	0.13E+04	0.98E+03	0.16E+04	0.16E+04	0.62E+03	0.10E+04	0.00E+00	0.38E+03
SVE100			0.64E+03	0.48E+03	0.19E+04	0.11E+04	0.10E+04	0.27E+04	0.91E+02	0.73E+03	0.22E+04	0.00E+00

Top table (T)

1 10 T	MIS080	MIS085	MIS090	MIS095	MIS100	SVE080	SVE085	SVE090	SVE095	SVE100
MIS080	0.00E+00	0.12E+05	0.58E+04	0.18E+05	0.12E+05	0.12E+05	0.23E+05	0.20E+05	0.42E+05	0.24E+05
MIS085	0.12E+05	0.00E+00	0.24E+05	0.12E+05	0.21E+05	0.24E+05	0.21E+05	0.26E+05	0.37E+05	0.44E+05
MIS090	0.58E+04	0.24E+05	0.00E+00	0.26E+05	0.91E+04	0.15E+05	0.34E+05	0.36E+05	0.58E+05	0.31E+05
MIS095	0.18E+05	0.12E+05	0.26E+05	0.00E+00	0.24E+05	0.24E+05	0.31E+05	0.27E+05	0.46E+05	0.41E+05
MIS100	0.12E+05	0.21E+05	0.91E+04	0.24E+05	0.00E+00	0.12E+05	0.26E+05	0.35E+05	0.39E+05	0.42E+05
SVE080	0.12E+05	0.24E+05	0.15E+05	0.24E+05	0.12E+05	0.00E+00	0.17E+05	0.21E+05	0.35E+05	0.29E+05
SVE085	0.23E+05	0.21E+05	0.34E+05	0.31E+05	0.26E+05	0.17E+05	0.00E+00	0.34E+05	0.14E+05	0.46E+05
SVE090	0.20E+05	0.26E+05	0.36E+05	0.27E+05	0.35E+05	0.21E+05	0.34E+05	0.00E+00	0.67E+05	0.30E+05
SVE095	0.42E+05	0.37E+05	0.58E+05	0.46E+05	0.39E+05	0.35E+05	0.14E+05	0.67E+05	0.00E+00	0.74E+05
SVE100	0.24E+05	0.44E+05	0.31E+05	0.41E+05	0.42E+05	0.29E+05	0.46E+05	0.30E+05	0.74E+05	0.00E+00

Bottom table (F)

1 10 F	MIS080	MIS085	MIS090	MIS095	MIS100	SVE080	SVE085	SVE090	SVE095	SVE100
MIS080	0.00E+00	0.13E+04	0.21E+04	0.26E+04	0.62E+03	0.12E+04	0.29E+04	0.71E+04	0.13E+05	0.78E+04
MIS085	0.13E+04	0.00E+00	0.22E+04	0.17E+04	0.21E+04	0.15E+04	0.18E+04	0.44E+04	0.92E+04	0.54E+04
MIS090	0.21E+04	0.22E+04	0.00E+00	0.18E+04	0.22E+04	0.37E+04	0.17E+04	0.49E+04	0.99E+04	0.66E+04
MIS095	0.26E+04	0.17E+04	0.18E+04	0.00E+00	0.17E+04	0.18E+04	0.91E+03	0.22E+04	0.56E+04	0.32E+04
MIS100	0.62E+03	0.21E+04	0.22E+04	0.17E+04	0.00E+00	0.12E+04	0.26E+04	0.66E+04	0.12E+05	0.73E+04
SVE080	0.12E+04	0.15E+04	0.37E+04	0.18E+04	0.12E+04	0.00E+00	0.19E+04	0.49E+04	0.95E+04	0.49E+04
SVE085	0.29E+04	0.18E+04	0.17E+04	0.91E+03	0.26E+04	0.19E+04	0.00E+00	0.24E+04	0.58E+04	0.31E+04
SVE090	0.71E+04	0.44E+04	0.49E+04	0.22E+04	0.66E+04	0.49E+04	0.24E+04	0.00E+00	0.32E+04	0.31E+04
SVE095	0.13E+05	0.92E+04	0.89E+04	0.56E+04	0.12E+05	0.95E+04	0.50E+04	0.32E+04	0.00E+00	0.15E+04
SVE100	0.78E+04	0.54E+04	0.66E+04	0.32E+04	0.73E+04	0.49E+04	0.31E+04	0.31E+04	0.15E+04	0.00E+00

APPENDIX C
HYPERLINE DERIVATION

Data from a frequency scan on a target defines a vector* in multidimensional space.

$$V'_p(\alpha) = x_{p1}(\alpha)\hat{i}_1 + x_{p,2}(\alpha)\hat{i}_2 + \ldots + x_{pn}(\alpha)\hat{i}_n$$

        p^{th} target

        n components (or dimensions)

           (1 or 2 components per frequency in the case of the ship data)

$V'_p(\alpha)$ will trace a line. Assume a fit to a straight line is meaningful.

$$V_p(\alpha) = M_p\alpha + B_p$$

where:

$$M_p = m_{p1}\hat{i}_1 + m_{p2}\hat{i}_2 + \ldots + m_{pn}\hat{i}_n$$

$$B_p = b_{p1}\hat{i}_1 + b_{p2}\hat{i}_2 + \ldots + b_{pn}\hat{i}_n$$

The distance between two points on two lines:

$$d_{1,2}(\alpha_1,\alpha_2) = |V_1(\alpha_1) - V_2(\alpha_2)|$$

The skew angle $\phi_{1,2}$:

$$\cos\phi_{1,2} = \frac{M_1 \cdot M_2}{|M_1| \cdot |M_2|}$$

If V_1 and V_2 are "good" estimates of V'_1 and V'_2, then d_{12} and ϕ_{12} are measures of the classification potential of V'_1 versus V'_2.

———————————

*All vectors in this appendix are capatalized. All scalars are small letters.

$|D| = d$ is minimum when:

$$D \cdot M_1 = 0 \text{ and } D \cdot M_2 = 0$$

$$D = V_1 - V_2$$

$$V = M\alpha + B$$

$$(V_1 - V_2) \cdot M_1 = V_1 \cdot M_1 - V_2 \cdot M_1 = 0$$

Thus: [Scalars]

$$(M_1 \cdot M_1)\alpha_1 - (M_2 \cdot M_1)\alpha_2 + (B_1 - B_2) \cdot M_1 = 0$$

$$(M_1 \cdot M_2)\alpha_1 - (M_2 \cdot M_2)\alpha_2 + (B_1 - B_2) \cdot M_2 = 0$$

At this point, there are two scalar equations in two unknowns (α_1 and α_2).

SO: Find α_1 and α_2

Gives d minimum and ϕ.

ATE
LMED
-8